iScience

CellPress
OPEN ACCESS

Article

Heme oxygenase-1 mitigates liver injury and fibrosis via modulation of LNX1/Notch1 pathway in myeloid cells

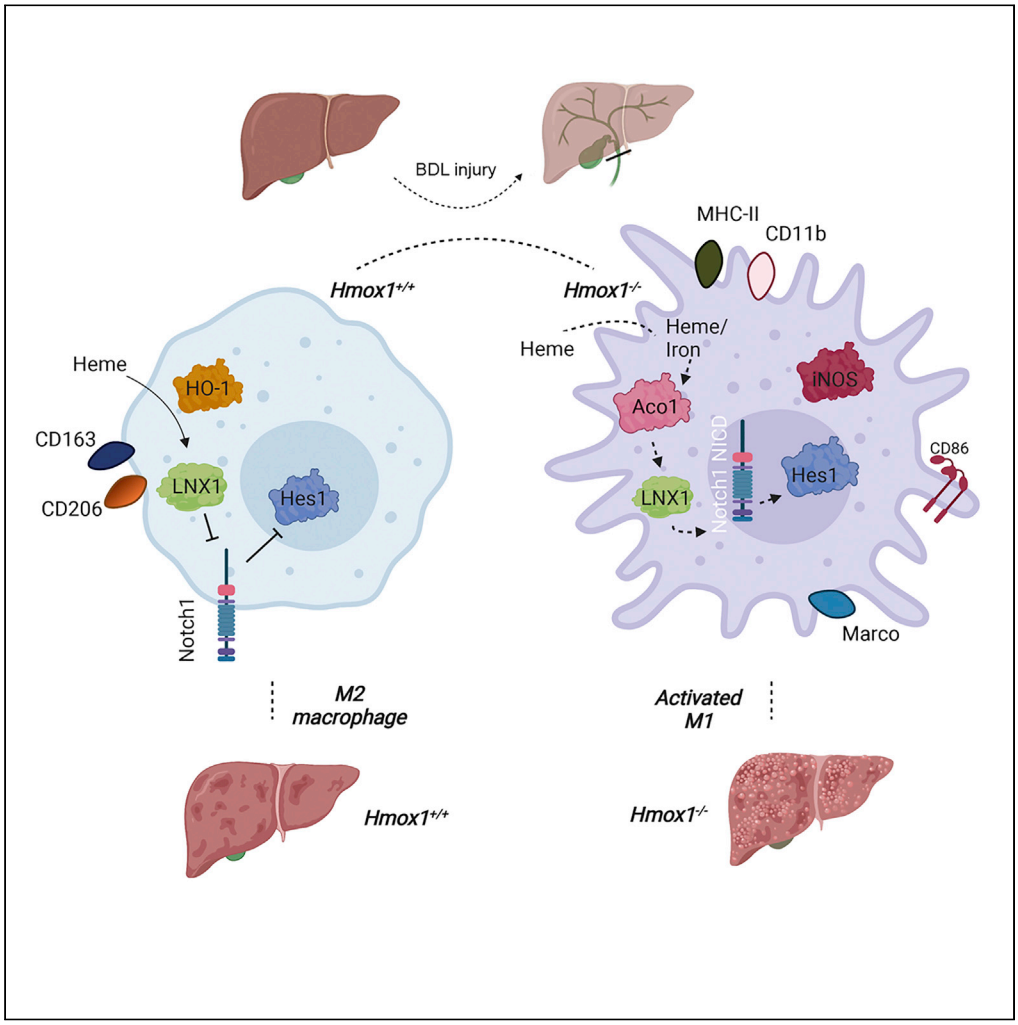

Giacomo Canesin, Linda Feldbrügge, Guangyan Wei, ..., Imad Nasser, Yury V. Popov, Barbara Wegiel

ypopov@bidmc.harvard.edu (Y.V.P.)
bwegiel@bidmc.harvard.edu (B.W.)

Highlights

Deletion of HO-1 in myeloid cells promotes liver injury and fibrosis

HO-1 supports M2-like polarization of macrophages in the liver

HO-1 modulates Notch1 signaling through ligand of numb-protein X1 (LNX1)

Canesin et al., iScience 25, 104983
September 16, 2022
https://doi.org/10.1016/j.isci.2022.104983

iScience

CellPress
OPEN ACCESS

Article

Heme oxygenase-1 mitigates liver injury and fibrosis via modulation of LNX1/Notch1 pathway in myeloid cells

Giacomo Canesin,[1,10,12] Linda Feldbrügge,[2,3,12] Guangyan Wei,[3,4,12] Lubica Janovicova,[1,5] Monika Janikova,[1,5] Eva Csizmadia,[1] Juliana Ariffin,[1] Andreas Hedblom,[1] Zachary T. Herbert,[6] Simon C. Robson,[7] Peter Celec,[5] Kenneth D. Swanson,[8] Imad Nasser,[9] Yury V. Popov,[3,11,*] and Barbara Wegiel[1,10,11,13,*]

SUMMARY

Activation of resident macrophages (Mϕ) and hepatic stellate cells is a key event in chronic liver injury. Mice with heme oxygenase-1 (HO-1; *Hmox1*)-deficient Mϕ (*LysM-Cre:Hmox1$^{fl/fl}$*) exhibit increased inflammation, periportal ductular reaction, and liver fibrosis following bile duct ligation (BDL)-induced liver injury and increased pericellular fibrosis in NASH model. *RiboTag*-based RNA-sequencing profiling of hepatic HO-1-deficient Mϕ revealed dysregulation of multiple genes involved in lipid and amino acid metabolism, regulation of oxidative stress, and extracellular matrix turnover. Among these genes, ligand of numb-protein X1 (*LNX1*) expression is strongly suppressed in HO-1-deficient Mϕ. Importantly, HO-1 and LNX1 were expressed by hepatic Mϕ in human biliary and nonbiliary end-stage cirrhosis. We found that Notch1 expression, a downstream target of LNX1, was increased in *LysM-Cre:Hmox1$^{fl/fl}$* mice. In HO-1-deficient Mϕ treated with heme, transient overexpression of *LNX1* drives M2-like Mϕ polarization. In summary, we identified LNX1/Notch1 pathway as a downstream target of HO-1 in liver fibrosis.

INTRODUCTION

Liver fibrosis is a feature of most chronic liver diseases and is currently one of the major causes of mortality and morbidity in Western countries (Asrani et al., 2019; Williams et al., 2018). This disorder most often results from chronic liver injury, such as alcoholic liver disease, non-alcoholic steatohepatitis (NASH) (Tsuchida and Friedman, 2017), or bile duct obstruction. It is characterized by the progressive deposition of extracellular matrix (ECM) proteins by activated hepatic stellate cells (HSC), the main fibrogenic effector cell type in the liver (Tag et al., 2015). Although liver fibrosis is potentially reversible during early stages, many cases progress to cirrhosis, which is difficult to treat and increases the risk of developing life-threatening sequelae such as hepatocellular carcinoma (HCC) or mixed cholangiocarcinoma (Ellis and Mann, 2012; Llovet and Bruix, 2008). Profibrogenic HSC activation and proliferation of cholangiocytes/adult hepatic progenitors (collectively termed "ductular reaction") are key cellular processes driving liver fibrosis progression (Mederacke et al., 2013; Peng et al., 2016).

Heme oxygenase-1 (HO-1, encoded by *Hmox1*) is the main heme catabolic enzyme, for degrading free heme to iron, carbon monoxide (CO), and biliverdin (BV), with the latter being rapidly converted to bilirubin (BR) by biliverdin reductase (BLVR-A) (Canesin et al., 2020b; Wegiel et al., 2013). *Hmox1* expression can be induced in different tissues at both transcriptional and translational levels by multiple stimuli, including cellular stress, UV radiation, heavy metals, inflammation, and its own substrate, heme (Keyse and Tyrrell, 1989). The liver plays a crucial role for the body's iron homeostasis and systemic inflammation, and hepatic HO-1 is important for the regulation of both systems. The liver and spleen Mϕ exhibit constitutively high levels of HO-1 activity and *Hmox-1* expression under homeostatic conditions (Hedblom et al., 2019). The role of HO-1 in liver disease has been related mainly to its immunologically protective roles, as the metabolic signaling related to heme degradation has been strongly linked to improved liver pathology and better function (Vijayan et al., 2018).

[1]Department of Surgery, Division of Surgical Sciences, Beth Israel Deaconess Medical Center, Harvard Medical School, Boston, MA 02215, USA

[2]Charité – Universitätsmedizin, Corporate Member of Freie Universität Berlin and Humboldt-Universität zu Berlin, Department of Surgery, Campus Charité Mitte and Campus Virchow-Klinikum, 13353 Berlin, Germany

[3]Department of Medicine, Division of Gastroenterology, Hepatology and Nutrition, Beth Israel Deaconess Medical Center, Harvard Medical School, Boston, MA 02215, USA

[4]Department of Radiation Oncology, First Affiliated Hospital, Sun Yat-sen University, 510080 Guangzhou, China

[5]Institute of Molecular Biomedicine, Comenius University in Bratislava, 811 08 Bratislava, Slovakia

[6]Molecular Biology Core Facilities, Dana-Farber Cancer Institute, Boston, MA 02215, USA

[7]Department of Anesthesia, Beth Israel Deaconess Medical Center, Harvard Medical School, Boston, MA 02215, USA

[8]Department of Neurology, Beth Israel Deaconess Medical Center, Harvard Medical School, Boston, MA 02215, USA

[9]Department of Pathology, Beth Israel Deaconess Medical Center, Harvard Medical School, Boston, MA 02215, USA

[10]Present address: Vor Biopharma, 100

Continued

In NASH patients, HO-1 expression is significantly increased and correlates with the severity of the disease (Malaguarnera et al., 2005). Experimental models used to evaluate impacts of HO-1 on liver injury and scarring have given mixed results. Inhibition of HO-1 can enhance lipogenesis and collagen production, thus increasing liver fibrosis (Raffaele et al., 2019; Wang et al., 2013). Interestingly, although the induction of HO-1 by cobalt protoporphyrin IX (CoPP) prevented the progression of fibrosis in the *Mdr2*-null mouse model (Barikbin et al., 2012), this intervention has been shown to promote fibrosis after bile duct ligation (BDL) (Froh et al., 2007). In addition, the overexpression of HO-1 significantly inhibited the development of micronodular cirrhosis in a carbon tetrachloride (CCL4)-induced liver fibrosis model, also reducing Mϕ infiltration and HSC activation (Tsui et al., 2006).

We hypothesized that HO-1 activity leads to altered gene expression and phenotype, preferentially in Mϕ within the liver that support immune protection against tissue damage and fibrotic responses. We demonstrated activation/M1-like polarization of Mϕ with exacerbated liver damage and fibrosis in response to BDL-mediated injury in mice with myeloid conditional deletion of *Hmox1*. By using *RiboTag*-based sequencing, we identified a regulatory LNX1/Notch1 pathway downstream of HO-1 that drives a protective form of M2 polarization of Mϕ and inhibits expansion of reactive cholangiocytes and liver fibrosis.

RESULTS

HO-1$^+$ Mϕ protect against liver injury, ductal reaction, and fibrosis induced by BDL surgery

To investigate the role of HO-1 expressed in Mϕ during liver fibrosis progression, we subjected *Hmox1*$^{fl/fl}$ and *LysM-Cre:Hmox1*$^{fl/fl}$ mice to BDL surgery (Figure 1). HO-1 levels were primarily increased in Mϕ but not in hepatocytes as shown by immunohistochemical staining of livers from the BDL-operated mice (Figures 1A and 1B). These livers exhibited cholestasis, hepatocyte necrosis, hepatomegaly, and liver fibrosis (Figures 1C–1H). HO-1 loss in Mϕ resulted in increased expression of E-cadherin, a marker of reactive bile ducts in liver fibrosis models, in livers from both naive and BDL-treated mice (Figure 1B). The deletion of *Hmox1* in Mϕ also resulted in significant increase in relative liver sizes compared with *Hmox1*$^{fl/fl}$ mice at 11 and 17 days following BDL surgery (Figure 1C). Livers harvested from *LysM-Cre:Hmox1*$^{fl/fl}$ mice at this time point also exhibited larger necrotic and fibrotic areas, as determined biochemically via hydroxyproline level quantitation (Figure 1D), hematoxylin/eosin (Figures 1E and 1F), as well as quantitative morphometry of collagen proportional area in Sirius red staining (Figures 1G and 1H). mRNA levels of the fibrosis-related genes, collagen (*COL1*), *TGFβ*, and *Acta2* in livers were higher in both *Hmox1*$^{fl/fl}$ and *LysM-Cre:Hmox1*$^{fl/fl}$ mice after BDL surgery but their levels did not differ between the strains under either conditions (Figures 2A–2C). Importantly, animals lacking HO-1 in Mϕ showed an increased number of bile ducts in their livers at 17 days after BDL surgery, as indicated by higher numbers of E-cadherin- and cytokeratin-19 (CK-19)-expressing bile ducts (Figures 2D–2G). These data suggest that HO-1 expressed by myeloid cells suppresses excessive ductular reaction and fibrotic responses to cholestatic liver injury, unlike general overexpression of HO-1 by CoPP induction, which is deleterious (Froh et al., 2007).

Lack of HO-1 in myeloid cells alters Mϕ phenotype in the liver

To understand the mechanisms behind the protective role of Mϕ-expressed HO-1 in the BDL model, we employed the *RiboTag* technology to specifically analyze the gene expression profile of *Hmox1*-deficient Mϕ. This approach allows efficient isolation of ribosome-associated mRNAs from specific cell types based on Cre-driven expression that drives tissue-specific expression of an HA-tagged ribosome transgene (Sanz et al., 2009). We bred *LysM-Cre:RiboTag* mice to *Hmox1*$^{fl/fl}$ mice and obtained animals with conditional deletion of *Hmox1* in myeloid cells and concomitant myeloid-specific ribosome epitope-tagging (*LysM-Cre:Hmox1*$^{fl/fl}$*:RiboTag* mice) (Figure 3A). *LysM-Cre:RiboTag wild-type* mice were used as controls. Overall, response to BDL surgery was phenotypically similar in *LysM-Cre:RiboTag wild-type* mice and the *Hmox1*$^{fl/fl}$ parental strains (Figure S1). The *RiboTag* strategy enabled a 20- to 30-fold enrichment in the expression of the Mϕ markers: CD11b, H2-Ab (MHC-II), and CD206 (a.k.a. MMR, mannose receptor) compared with input RNA isolated from the total liver lysates (Figure 3B), demonstrating a high efficiency in myeloid-RNA enrichment. The same *Ribotag* analysis of RNA isolated from liver Mϕ after BDL surgery confirmed elevated *Hmox1* expression in control animals after BDL injury and the complete deletion of *Hmox1* gene in Mϕ in *LysM-Cre:Hmox1*$^{fl/fl}$*:RiboTag* mice (Figure 3C). A similar pattern of expression was observed for the second enzyme in heme degradation pathway, biliverdin reductase-A (*BLVR-A*), indicating regulation of this gene by HO-1 in Mϕ (Figure 3D). Levels of hemopexin (Hx), a heme scavenger, remained unchanged under all conditions, suggesting that its regulation is independent of heme metabolism in the liver (Figure 3E). Furthermore, selective deletion of HO-1 in Mϕ resulted in increased activation and pro-inflammatory

Cambridgepark Dr, Suite 400, Cambridge, MA 02140, USA

[11]Senior author

[12]These authors contributed equally

[13]Lead contact

*Correspondence: ypopov@bidmc.harvard.edu (Y.V.P.), bwegiel@bidmc.harvard.edu (B.W.)

https://doi.org/10.1016/j.isci.2022.104983

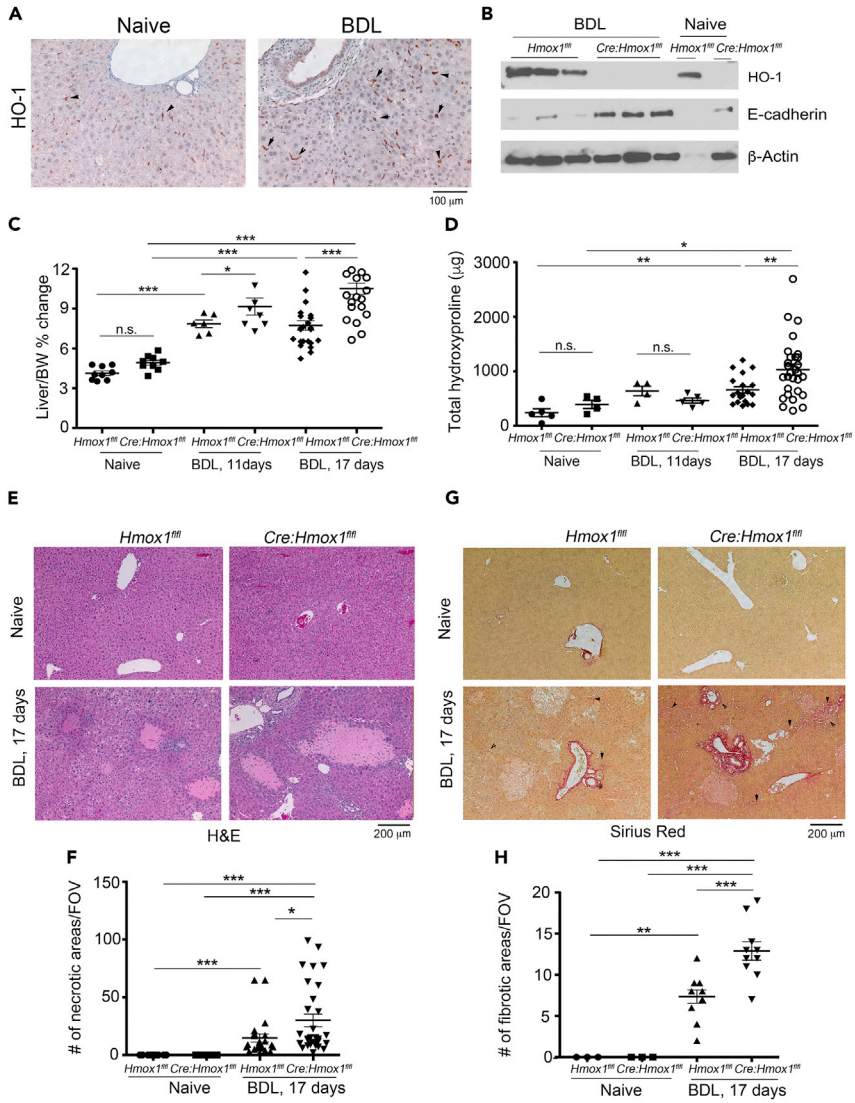

Figure 1. The role of myeloid-cell-expressed HO-1 in the BDL murine model of liver fibrosis

(A) Immunohistochemical (IHC) staining with antibodies against HO-1 in the liver samples from control and BDL-treated mice showing staining in sinusoidal macrophages. Scale bar: 100 μm.

(B) Western blot analysis of HO-1 and E-cadherin expression in liver lysates from mice untreated (naive) or subjected to BDL surgery (17 days post-surgery, BDL).

(C) Percentage of liver weights change per body weights (BW) of *Hmox1*$^{fl/fl}$ (WT) or *LysM-Cre:Hmox1*$^{fl/fl}$ (KO) mice, which were untreated or subjected to BDL surgery, 11 or 17 days post-surgery. ANOVA, $p < 0.0001$, Student's t test: ***$p < 0.001$, *$p < 0.05$. Data are represented as mean ± SEM n = 5–18 female and male mice per group.

(D) Hydroxyproline levels in the livers exposed to BDL surgery as described in (A) and harvested 17 days after BDL. ANOVA, $p = 0.0376$, Student's t test: *$p < 0.05$, **$p < 0.01$. Data are represented as mean ± SEM.

(E–H) Lobular necrosis (H &E, E) and fibrosis (Sirius red, G) in the livers from mice treated as in (A). Representative sections are shown from BDL-treated mice in (E) and (G) (100x magnification) and quantification of the data is presented in (F) and (H). Data are represented as mean ± SEM. ANOVA, $p < 0.0001$, Tukey's multiple comparison test: **$p < 0.01$, ***$p < 0.001$. Scale bar: 200 μm.

M1-like polarization of myeloid cells, as indicated by the higher relative levels of H2-Ab and iNOS expression, and reduction of M2 markers, including CD206 (MRC1, MMR), CD11b, and CD163, in both untreated and BDL-operated *LysM-Cre:RiboTag:Hmox1*$^{fl/fl}$ mice compared with their respective controls (*LysM-Cre:RiboTag)* (Figures 3F–3J). These data indicate a possible phenotypic change in Mϕ that may impact the progression of liver fibrosis in BDL model in the absence of HO-1.

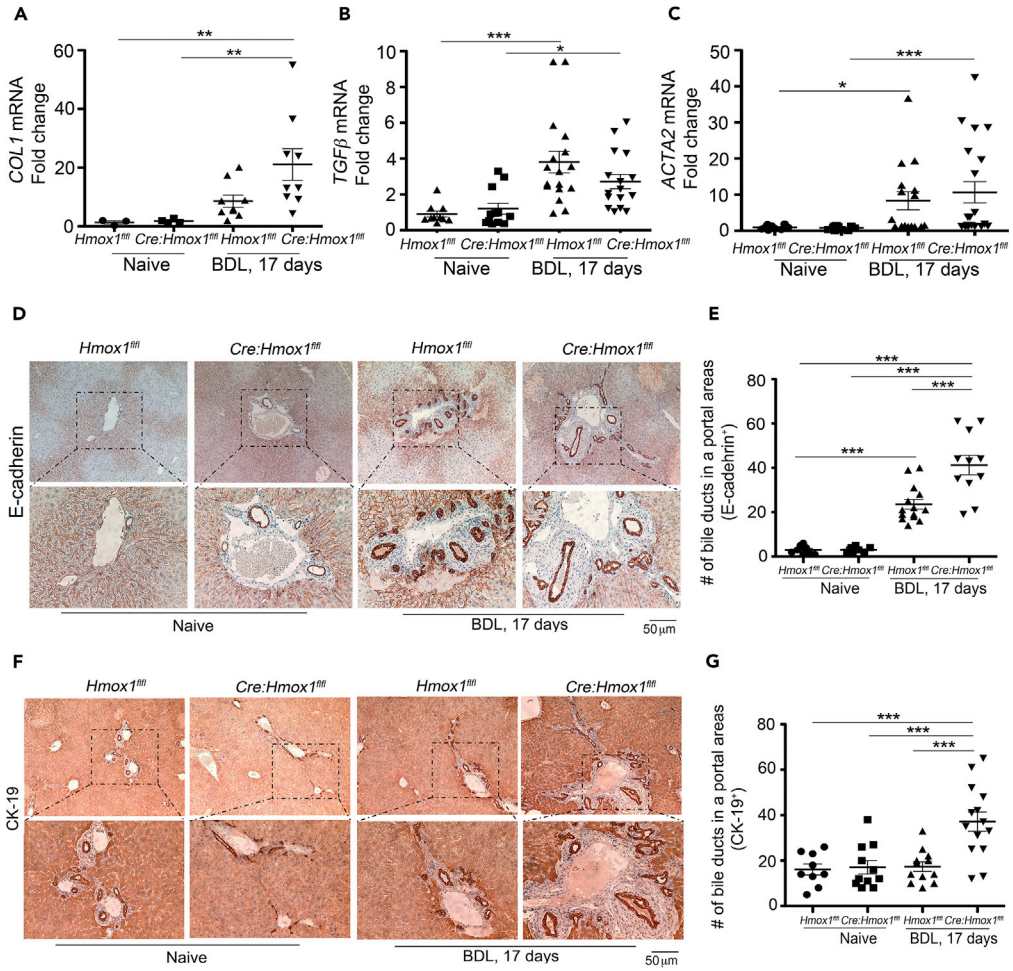

Figure 2. Deletion of HO-1 in macrophages leads to enhanced ductal reaction

(A–C) RT-PCR using the total liver mRNA and primers for *COL1* (A), *TGFβ* (B), and *ACTA2* (C). Data are represented as mean ± SEM. ANOVA, $p < 0.0001$, Tukey's multiple comparison test: *$p < 0.05$, **$p < 0.01$, ***$p < 0.001$.

(D–G) IHC staining with antibodies against E-cadherin (D) or CK-19 (F) in the liver samples from control and BDL-treated mice. Magnification of 200× (upper panels) or 400x (lower panels). Quantification of the data is shown in (E) and (G). Data are represented as mean ± SEM. ANOVA, $p < 0.0001$, Tukey's multiple comparison test: ***$p < 0.001$. Scale bar: 50 μm.

Myeloid gene expression measured by RiboTag RNA sequencing

By performing RNA-seq on RNA isolated from liver Mϕ using the *RiboTag* strategy we found significant changes in the expression of 3,300 genes at 17 days post-surgery in livers with significant fibrosis. Further, in HO-1-deficient mice, 250 genes exhibited altered expression in Mϕ from unoperated animals and an additional 55 genes showed altered expression in response to BDL treatment (Figure 4A). By gene ontology analysis, we demonstrated decreases in organic acid, lipid, and amino-acid-metabolism-related gene expression and an increase in acute inflammatory response genes in unchallenged *Hmox1*-deficient Mϕ (Figures S2A and S2B). These differences in gene expression signature seen after BDL surgery were further exacerbated in resident macrophages of mouse livers from *Hmox1*-deficient mice Mϕ measured at 17 days following BDL operation (Figure S2C). Further, BDL-driven response led to increased expression of genes involved in extracellular matrix organization and cell junctions, which were further upregulated in the absence of HO-1 in Mϕ in this model (Figures S2D–S2F), suggesting a role for heme metabolism in regulation of fibrotic responses.

qPCR analysis of genes identified by RNA-seq revealed that Lipocalin-2 (*Lcn2*), whose expression is induced in hepatic inflammation (Asimakopoulou et al., 2016), was significantly elevated in BDL-treated livers but was unaffected by *Hmox1* deletion (Figure 4B). We also identified two other genes as putative

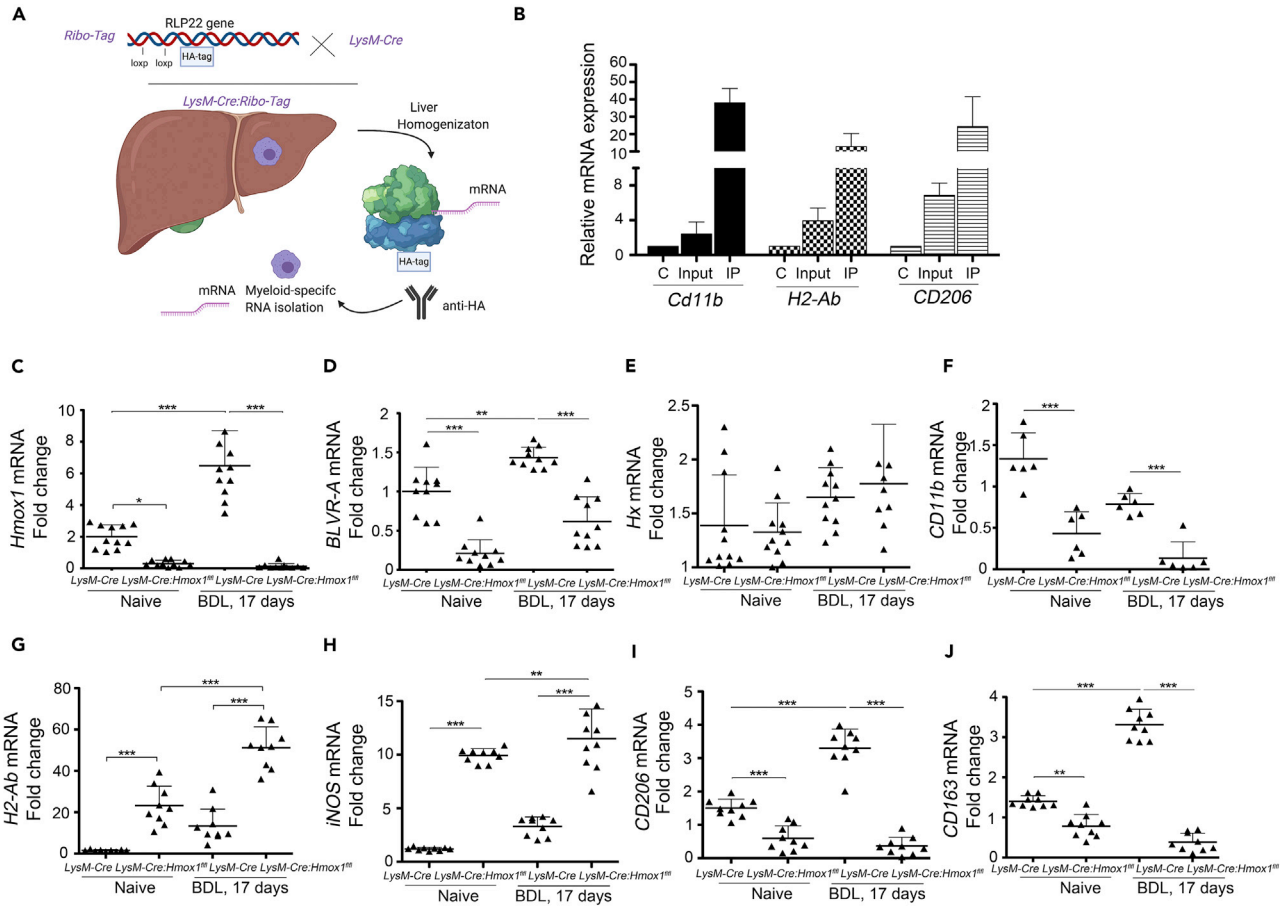

Figure 3. Deletion of HO-1 in myeloid cells impacts Mφ phenotype as assessed by *RiboTag* approach

(A and B) Liver lysates from *LysM-Cre:RiboTag* mice were subjected to immunoprecipitation (IP) with anti-HA antibody. A scheme of the technology is shown in (A). Myeloid markers were assessed by RT-PCR and are shown in (B). Data are represented as mean ± SEM.

(C–J) *LysM-Cre:RiboTag* or *LysMCre:Hmox1*$^{fl/fl}$*:RiboTag* mice were subjected to BDL surgery as described in Figure 1. RT-PCR was performed on the RNA from the IP with anti-HA antibody. Data are represented as mean ± SEM. ANOVA, $p < 0.0001$, Tukey's multiple comparison test: ***$p < 0.001$, **$p < 0.01$. n = 5–18 female and male mice per group.

targets of HO-1 in Mϕ: SULT2A8 and GPNMB (Figures 4C and 4D). The basal expression level of SULT2A8, a sulfotransferase for bile acids regulated by PPARα (Feng et al., 2017), was increased in the absence of HO-1 in Mϕ, but in response to BDL, its induction was significantly lower compared with that seen in wild type (WT) animals (Figure 4C). Interestingly, we found that GPNMB, which encodes the glycoprotein Nmb and whose expression and function were previously shown to be important for Mϕ function and phagocytosis in the context of ischemic injury (Li et al., 2010), was unaltered in Mϕ lacking HO-1 under baseline conditions but was significantly upregulated in response to BDL surgery compared with control animals (Figure 4D). A similar trend toward hyperactivity was observed for CD14 in *Hmox1*-deficient Mϕ following BDL surgery (Figure 4E). Consistent with our previous *ex vivo* data, the expression of Marco, an innate marker of Mϕ activation, was also increased in HO-1-deficient Mϕ in the livers of both unchallenged and BDL-operated mice (Figure 4F). Importantly, we identified a new HO-1 target, ligand of numb-protein X-1 (*LNX1*), whose mRNA expression was significantly decreased in HO-1-deficient Mϕ in both the basal state and in response to BDL surgery (Figure 4G).

To test whether LNX1 may be a target of HO-1 at the protein level, we performed IHC staining of liver sections and probed Western blots of whole liver lysates with antibodies against LNX1 (Figures 4H–4K). Interestingly, we detected low levels of LNX1 expression in infiltrating cells and hepatocytes in naive mice but significantly higher LNX1 protein levels in both cell types in the livers from Mϕ lacking HO-1 in response to BDL (Figures 4H–4J). A similar pattern of expression was seen on the Western blots (Figure 4K). Because

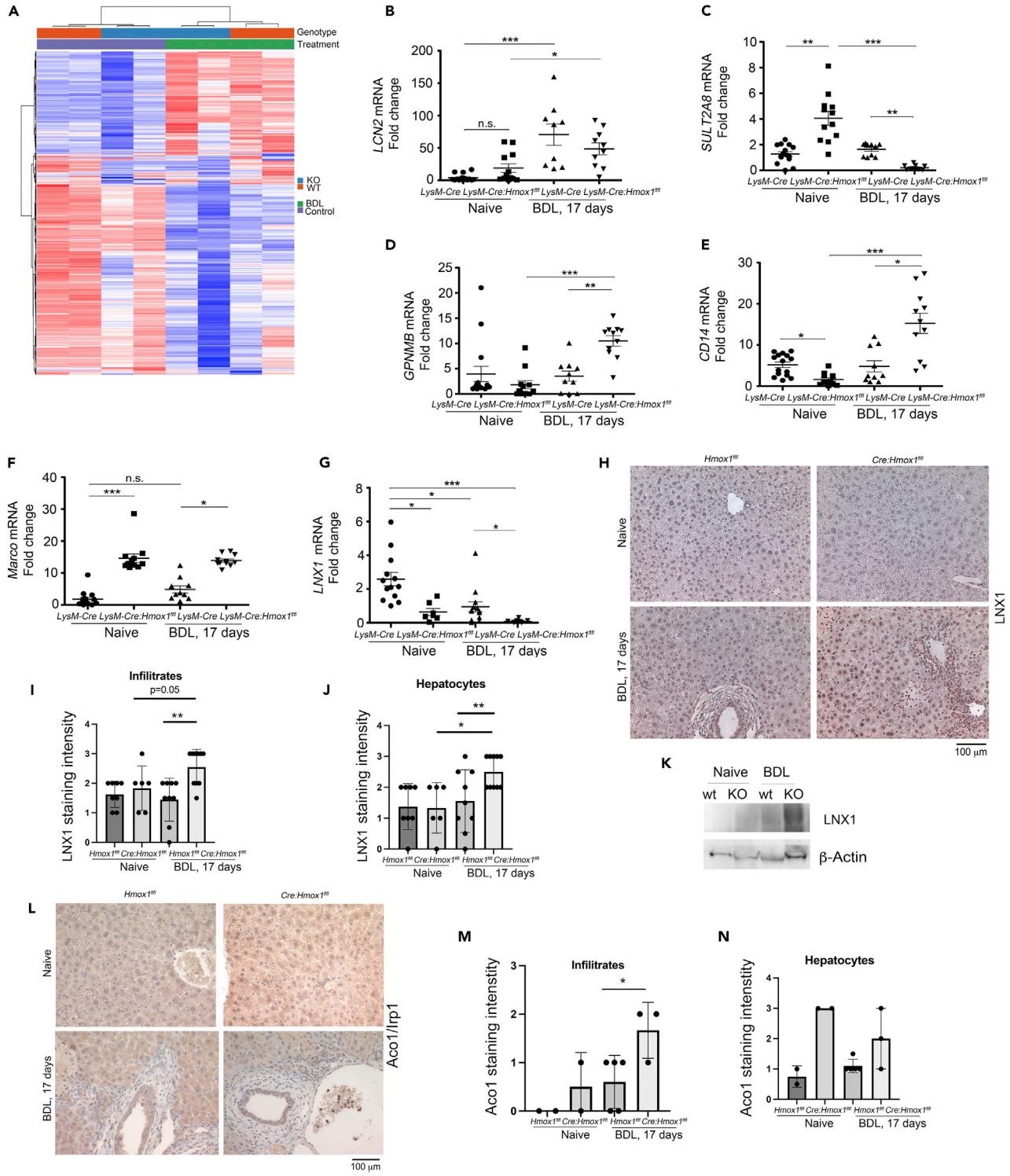

Figure 4. LNX1 is the HO-1 target gene in myeloid cells

(A) Gene clustering based on the RNA-seq on the RNA obtained from the IP with anti-HA antibody from the liver lysates of *LysM-Cre:RiboTag* (WT) and *LysMCre:Hmox1*$^{fl/fl}$*:RiboTag* (HO-1^{KO-M}) subjected to BDL surgery as in Figure 1. n = 2 mice per group.

(B–G) Confirmatory RT-PCR using the RNA isolated as in (A), assessing the top target genes as identified by RNA-seq (17 days after BDL). Data are represented as mean ± SEM. ANOVA, $p < 0.0001$, Dunn's multiple comparison test: ***$p < 0.001$, **$p < 0.01$, *$p < 0.05$. n = 5–18 female and male mice per group.

Figure 4. *Continued*

(H–J) Immunohistochemical staining of LNX1 in the liver samples from control and BDL-treated mice. Quantification of the data is shown in (I) and (J). Data are represented as mean ± SD. ANOVA, $p < 0.01$, Student's t test: $^{**}p < 0.01$, $^{*}p < 0.05$. Scale bar: 100 μm.

(L–N) Immunohistochemical staining of Aco1/Irp1 in the liver samples from control and BDL-treated mice. Quantification of the data is shown in (I) and (J). Data are represented as mean ± SD. ANOVA, $p < 0.01$, Student's t test: $^{*}p < 0.05$. Scale bar: 100 μm.

LNX1 mRNA has been recognized as a possible posttranscriptional target of Aco1/Irp1 (Sanchez et al., 2011), we have assessed the levels of Aco1/Irp1 in the BLD-treated livers (Figures 4L–4N). There was a significant increase in the Aco1/Irp1 protein levels in the infiltrating cells of KO mice, with the most pronounced expression in the livers from mice with Mϕ lacking HO-1 in response to BDL (Figures 4L–4M).

Because Aco1/Irp1 is a critical regulator of iron homeostasis in cells and complete deficiency of HO-1 results in accumulation of iron in the tissues, we assessed the iron levels in the livers by Prussian blue staining (Figure S3). We found a significant increase of iron accumulation in BDL-treated livers compared with naive mice; however, we did not see any statistical difference in the levels of iron between the genotypes under either condition (Figure S3). Based on the RNA-seq data, we did not see any difference in the ferroptosis genes (*Acsl4*, *Tfr*, *Ptgs2*, *Chac1*). Moreover, there was no difference in the Nrf2 expression, a master gene controlling oxidative stress and HO-1 expression, between the genotypes (Figure S4). Interestingly, Nrf2 was strongly expressed in Kupffer cells and infiltrating cells in naive mice but not in the BDL-treated livers (Figure S4).

Elevated expression of LNX1 in human biliary and non-biliary end-stage cirrhosis

To study the role of LNX1 downstream of HO-1 in Mϕ, we first assessed its hepatic expression along the staining with HO-1 by IHC in human liver fibrosis (Figures 5A–5D). Inflammatory cells expressed both HO-1 and LNX1 in human liver biopsies from NAFLD/NASH patients (n = 5) with advanced fibrosis (Figure 5A). LNX1 expression was also observed in the bile ducts and hepatocytes of NAFLD livers (Figure 5A). In the pilot analysis of stage-wise progression of NASH fibrosis (fibrosis stages: FS0 to FS3-4), we demonstrated redistribution of the HO-1 staining from pan-lobular localization in Kupffer cells to scar-associated cells infiltrating the interstitial fibrotic lesion. Further, more intense HO-1 staining was associated with presence of active NASH (defined as disease activity score NAS 4–8, as compared with lower NAS indicative of simple steatosis [0–3]) (Figure 5A). LNX1 staining primarily concentered within the reactive ducts and fibrotic lesions with overall higher staining in patients with more advanced fibrosis (Figure 5B). Further, we performed a survey of HO-1/LNX1 expression in human explant livers with end-stage liver disease due to various etiologies such as primary biliary cholangitis (PBC, n = 3), alcoholic liver disease (Alc, n = 5), or cryptogenic cirrhosis (Crypto, n = 5) (Figures 5B–5D). We have readily detected HO-1^{+} inflammatory cells in cirrhotic livers due to PBC and alcoholic disease, whereas lower numbers of HO-1^{+} cells (not inflammatory) were observed in cryptogenic liver fibrosis (Figures 5B and 5C). LNX1 immunopositivity marked infiltrating cells, hepatocytes, and bile ducts in all samples, with the highest abundance observed in cryptogenic liver fibrosis samples (Figures 5B and 5D). The expression of LNX1 in hepatocytes appeared faint compared with inflammatory cells or cholangiocytes (Figures 5C and 5D).

Because HO-1 expression was strongly positive in patients with NASH (Figure 5A), we fed mice deficient with myeloid-cell-specific deletion of *Hmox1* the methionine- and choline-deficient (MCD) diet for 3 weeks (murine NASH model) and evaluated them for fatty liver and fibrosis scores (Figures 5E–5G). Liver harvested from *LysM-Cre:Hmox1*$^{fl/fl}$ mice fed with MCD diet showed more fat accumulation and significantly more pericellular fibrosis compared with control mice on the same diet (Figures 5E–5G).

Analysis of LNX1 expression and its targets in HO-1-deficient Mϕ

In order to test whether heme-induced HO-1 plays a role in LNX1 expression, we assessed the levels of LNX1 protein in HO-1-deficient bone-marrow-derived Mϕ (BMDM) following heme treatment. We confirmed the complete deletion of the HO-1 on the protein level in HO-1-deficient bone-marrow-derived Mϕ (Figure 6A) as well as lack of toxicity of heme treatment in BMDM (Figure S5A). We found that basal LNX1 protein levels were not different in BMDM from both genotypes (Figure 6B), despite slightly increased mRNA levels of LNX1 in KO cells (Figure S5B). Although we found a significant induction of LNX1 at the protein level in response to heme (24 h) in BMDM from control mice (Figures 6B and 6C), heme treatment did not result in increased levels of *LNX1* mRNA (Figure S5B). Interestingly, LNX1 levels were unchanged in response to heme in HO-1-deficient BMDM (Figures 6B and 6C). In addition, the levels

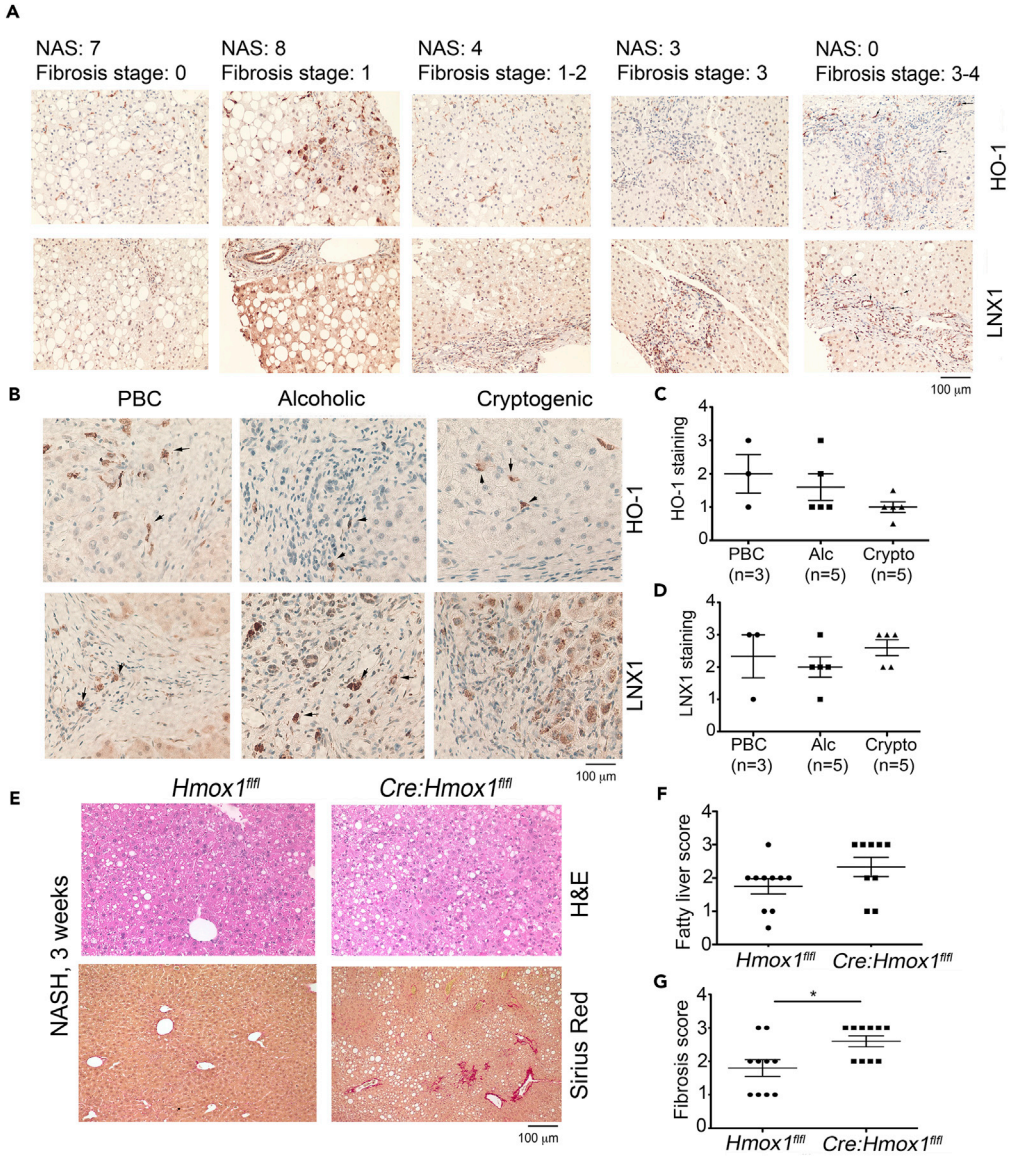

Figure 5. Detection of HO-1$^+$ and LNX1$^+$ cells in the human samples with increasing fibrosis stage and assessment of the role of HO-1 in myeloid cells in fibrosis progression in murine NASH model

(A–D) IHC staining with antibodies against LNX1 or HO-1 in (A) human liver biopsies from n = 5 patients with various stages of NAFLD/NASH with the clinical characteristic as described in STAR Methods. (B–D) Human liver explants obtained from patients undergoing orthotopic liver transplantation due to end-stage liver disease of various etiologies (n = 3 PBC, n = 5 Alc, n = 5 Crypt) (Peng et al., 2016). Representative staining in myeloid cells/macrophages is shown in (A) and (B). Scale bar: 100 μm (A) and 50 μm (B). Quantification of the HO-1$^+$ and LNX1$^+$ cells are shown in (C) and (D). Data are represented as mean ± SEM. ANOVA, not significant.

(E–G) *Hmox1*$^{fl/fl}$ (*Hmox1*$^{fl/fl}$) or *LysM-Cre:Hmox1*$^{fl/fl}$ (*Cre:Hmox1*$^{fl/fl}$) mice were fed with methionine- and choline-deficient (MCD) diet for 3 weeks. Livers were evaluated for fibrosis and fatty scores based on the Sirius red staining and H&E. Data are represented as mean ± SEM. Student's t test: *p < 0.05. n = 10 mice/group. Scale bar: 100 μm.

of Aco1/IRP1 were also increased by heme treatment in BMDM isolated from wild-type mice but remain unchanged in KO cells in response to heme (Figure 6B).

To further assess whether LNX1 is critical to the role of HO-1 in regulating Mϕ biasing toward the M2 phenotype, we genetically manipulated its expression in Mϕ with HO-1 knockdown followed by the heme treatment. Over-expression of *LNX1* by transfection in RAW264.7 Mϕ (Figures 6D–6G) led to changes in specific HO-1-regulated

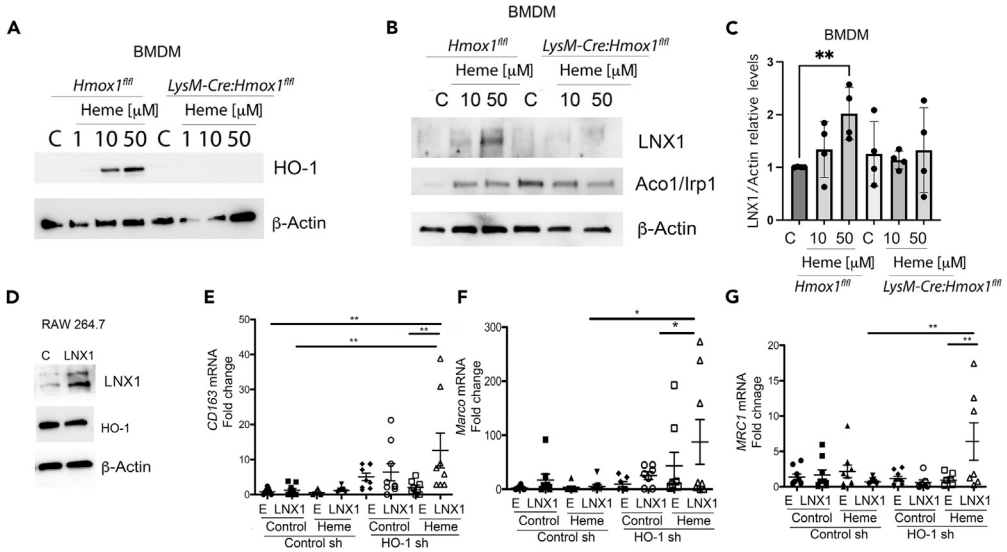

Figure 6. The role of LNX1 in Mφ

(A–C) Bone-marrow-derived Mφ (BMDM) were isolated from *Hmox1*$^{fl/fl}$ or *LysM-Cre:Hmox1*$^{fl/fl}$ and treated with heme (1–50 μM) for 24 h. Protein analyses were performed with antibodies against HO-1, LNX1, and Aco1/IRP1. Quantification of LNX1 expression is shown in (C). Data are represented as mean ± SEM. ANOVA, p = 0.144, Student's t test: **p < 0.01. (D–G) LNX1 was overexpressed in RAW264.7 Mφ by transient transfection. Western blot with antibody against LNX1 is shown in (D). RT-PCR analyses with indicated primers in the RAW264.7 Mφ with transient overexpression of LNX1 and treated with heme (50 μM) for 6 h are shown in (E–G). Data are represented as mean ± SEM. ANOVA, p < 0.01, Tukey's multiple comparison test: *p < 0.05, **p < 0.01.

genes in both unstimulated and heme-stimulated RAW264.7 Mφ with HO-1 knockdown (Figures 6D–6G and S5C). As expected, the level of HO-1 expression was increased upon heme challenge and attenuated in the RAW264.7 Mφ with stable knockdown of HO-1 (Figure S5D). Heme treatment of RAW264.7 cells with stable knockdown of HO-1 and overexpressing *LNX1* led to a significant increase in expression of several Mφ markers, including CD163, Marco, and CD206 (MRC1) (Figures 6E–6G), consistent with M2-like polarization.

Notch1 signaling as a target of HO-1 in Mφ

Because LNX1 regulates Notch1 (Baisiwala et al., 2020) and our previous studies indicated the crosstalk between HO-1 and the Notch1 pathway (Nemeth et al., 2016), we therefore assessed the role of LNX1 in Notch1 signaling in our model (Figure 7). At both 11 and 17 days after BDL surgery Mφ exhibited increased Notch1 expression and a significant increase in the number of Notch-1-positive Mφ in the livers of *LysM-Cre:Hmox1*$^{fl/fl}$ mice (Figures 7A and 7B). We also detected an increase in the basal levels of *Notch1* and *Hes1* mRNA in *LysM-Cre:Hmox1*$^{fl/fl}$ mice and BDL induced their expression in both *Hmox1*$^{fl/fl}$ and *LysM-Cre:Hmox1*$^{fl/fl}$ mice (Figures 7C and 7D). We also examined the levels of the *Hes-1*-regulated gene, *GATA-1*, a known inhibitor of IL-6-induced Mφ differentiation (Tanaka et al., 2000) and whose level was elevated in BDL-treated mice (Figure 7E). To assess the role of HO-1-modulated *LNX1* in regulating genes downstream of Notch1 activation, we analyzed the expression of *Notch1*, *Hes1*, and *GATA-1* in *LNX1*-overexpressing RAW264.7 Mφ (Figures S5F–S5H). *Notch1* mRNA remained unaffected by *LNX1* overexpression (Figure S5G). Knockdown of HO-1 in RAW264.7 Mφ resulted in slight increase in *GATA-1* expression but no changes in *Hes1* expression (Figures S5F–S5H). However, overexpression of *LNX1* in RAW264.7 Mφ with knockdown of HO-1 and stimulation with heme resulted in suppression of *Hes1* expression (Figure S5F). These data suggest the role of HO-1-mediated LNX1 regulation of Notch1 signaling.

DISCUSSION

In this study, we uncovered the role of HO-1 in determining hepatic macrophage fate by controlling Notch1 signaling through *LNX1* expression in Mφ. By employing a model of periportal/periductular liver fibrosis, we found increased Mφ activation and enhanced liver fibrosis in mice with Mφ-specific HO-1 deficiency. Further, myeloid-specific RNA sequencing using *RiboTag* labeling led to identification of previously unknown targets of HO-1 in Mφ, including *LNX1*, *SULT2A8*, *GPNMB*, and *Dab1*. Significantly, deletion of

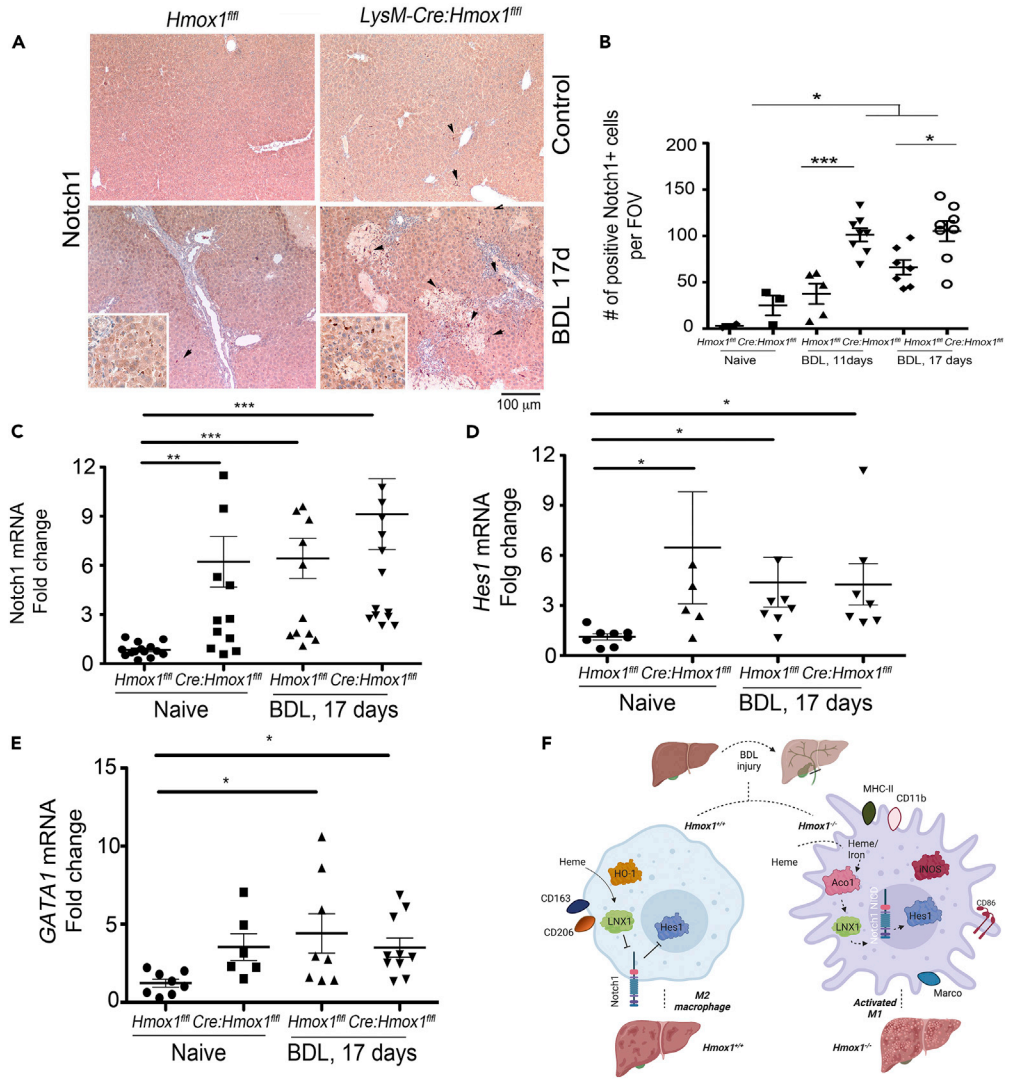

Figure 7. A crosstalk of HO-1 and Notch1 signaling in Mφ

(A and B) Immunostaining with antibody against Notch1 total was performed in the livers isolated from *Hmox1*$^{fl/fl}$ or *LysM-Cre:Hmox1*$^{fl/fl}$ (*Cre:Hmox1*$^{fl/fl}$) mice after BDL surgery. Scale bar: 100 μm (insets: 400x magnification). The quantification of a number of Notch1+ cells is shown in (B). Data are represented as mean ± SEM. ANOVA, $p < 0.001$, Tukey's multiple comparison test: *$p < 0.05$, ***$p < 0.001$.

(C–E) *LysM-Cre:RiboTag (Hmox1*$^{fl/fl}$*)* or *LysMCre:Hmox1*$^{fl/fl}$*: RiboTag* (*Cre:Hmox1*$^{fl/fl}$) mice were subjected to BDL surgery as in Figure 2. RT-PCR was performed using RNA isolated from the immunoprecipitates with the anti-HA antibody. Data are represented as mean ± SEM. ANOVA, $p < 0.0001$, Tukey's multiple comparison test: ***$p < 0.001$, **$p < 0.01$. n = 5–18 female and male mice per group.

(F) Scheme representing the interaction of LNX1 in HO-1 and regulation of Mφ phenotype during liver injury.

HO-1 promoted M1-like polarization of Mϕ, which was reversed by overexpression of *LNX1*, providing a first documentation of its role as the mediator acting downstream of HO-1 in the control of Mϕ phenotype (Figure 7H). We also provided evidence for the HO-1-dependent mechanism of determining Mϕ fate that at least in part involves the effect of LNX1 on Notch1 signaling pathway.

Despite growing interest in heme metabolism and HO-1 in liver physiology and pathology, there is a limited understanding of the mechanisms of HO-1 in the context of development and progression of liver fibrosis. Almost 20% of NAFLD patients present with inflammation and fibrosis (NASH, non-alcoholic steatohepatitis), which can lead to cirrhosis and hepatocarcinoma (Wei et al., 2020a). Inflammatory signals, such as danger-associated molecular patterns (i.e., mito-DAMPs or heme) released from injured hepatocytes

directly activate hepatic stellate cells to drive fibrosis, particularly in biliary disease (An et al., 2020; Wegiel et al., 2015). Heme is particularly toxic when released from hemoproteins either due to erythrocyte or other cell damage, leading to inflammation and oxidative stress (Lundvig et al., 2012). We hypothesized that heme metabolizing enzyme, HO-1, is a critical protective molecule against chronic inflammation, hepatic stellate cells activation, and liver scaring by turning on a specific gene expression profile in Mϕ due to removal of heme (Li et al., 2003). Notch1 signaling has not only been characterized as a driver of HSC activation, bile duct reaction, and fibrosis (Adams and Jafar-Nejad, 2019; Geisler and Strazzabosco, 2015) but also as a downstream target of heme metabolism (Nemeth et al., 2016). Here we show augmented Notch1 expression and activity in the livers of *LysM-Cre:Hmox1*$^{fl/fl}$ mice. HO-1 was shown to suppress Wnt signaling in NASH-related liver fibrosis (Boulter et al., 2012), which may oppose Notch1 activation (Boulter et al., 2012). Notch1 signaling is one of the regulators of Mϕ maturation and polarization toward M1-like phenotype (Monsalve et al., 2006; Weijzen et al., 2002) and a driver of liver fibrosis. The potential crosstalk between Notch1 and Wnt upon deletion of HO-1 will be addressed in future studies.

Heme metabolism is essential to maintain liver physiology, and HO-1 has been established as a critical enzyme and immunomodulator in liver function and pathology (Hedblom et al., 2019; Vijayan et al., 2018). Several studies have shown that blocking HO-1 can enhance lipogenesis and collagen production and increase liver fibrosis (Raffaele et al., 2019; Wang et al., 2013), whereas HO-1 induction can prevent the progression of liver fibrosis (Barikbin et al., 2012). Augmented HO-1 expression is beneficial for reducing inflammation and fibrosis in liver injury models through its enhanced antioxidant activity. Interestingly, some HO-1 inducers (i.e., curcumin, pomegranate seed oil, or resveratrol) are currently being studied as possible treatment for liver diseases characterized by lipid accumulation and fibrosis in NAFLD patients (Stec and Hinds, 2020).

Our data show that liver fibrosis in the BDL model is characterized by phenotypic changes in myeloid cells in the absence of HO-1. Mϕ lacking HO-1 show high expression of MHCII and iNOS and low levels of CD206 and CD163, which corresponds to M1-like phenotype skewing. A recent study showed that induction of HO-1 expression promotes a switch from M1- to M2-like Mϕ phenotype, resulting in the protection against liver ischemia-reperfusion injury (Naito et al., 2014; Zhang et al., 2018). Despite these findings about the role of HO-1 in acute liver injury, studies on the role of HO-1 in Mϕ phenotype in liver fibrosis are missing. It has been shown that induction of HO-1 expression significantly suppressed hepatic stellate cells activation and liver fibrosis in the *Mdr2* knockout model and was associated with lower immune cell infiltration to the liver (Barikbin et al., 2012). A study by Salley et al. showed that upregulation of HO-1 expression by hemin administration suppressed several pro-inflammatory cytokines and chemokines while potentiating the protein expression of anti-inflammatory M2-phenotype markers, which resulted in an attenuated liver injury and fibrosis (Salley et al., 2013). Our results corroborate these findings and indicate that a phenotypic change in Mϕ may impact the progression of liver fibrosis in the absence of HO-1. It is possible that HO-1 contributes to the phenotype of other myeloid cells such as neutrophils that are implicated in liver injury and fibrosis and cannot be excluded, as *LysM* promoter drives Cre in myeloid cells.

In this study, we defined gene expression profiles specifically in the Mϕ using the *RiboTag*-RNA-seq technology. We identified a broad spectrum of gene changes in Mϕ lacking HO-1 in response to BDL-induced liver fibrosis and several targets of HO-1 in Mϕ. Here we report identification of three HO-1 targets in Mϕ: *LNX1*, *SUL2A8*, and *GPNMB*. LNX1 is a ubiquitin-protein ligase, which has been recently identified as a regulator of Numb and Notch1 pathway (Baisiwala et al., 2020) but has not been studied in liver disease models. We found that *LNX1* mRNA levels were significantly suppressed in Mϕ in the liver in response to BDL as well as in Mϕ with HO-1 deletion, both basally and after BDL surgery. LNX1 regulation remains poorly understood, with a recent report suggesting a connection to the iron homeostasis. The genome-wide search for IRP1/Aco1-associated mRNAs revealed LNX1 mRNA binding to IRP1 and IRP2 (Sanchez et al., 2011). Because HO-1 metabolism is a source and regulator of intracellular iron, by modulating ferritin levels, the indirect regulation of LNX1 levels by IRP-1-mediated mechanism is plausible. Our data suggest a similar change in expression of LNX1 and IRP-1/Aco1 in the liver samples. However, the detailed mechanisms of LNX1 regulation by the HO-1 and heme metabolic pathways in various cell types need to be addressed in future studies. Further, there are several possible explanations of the difference in LNX1 levels between the liver macrophages versus BMDM *in vitro*. The *in vitro* conditions are different than *in vivo* where local heme levels and interaction with other cells may alter LNX1 levels in Mϕ Further, the difference in the interaction with other cell types, differential cytokine milieu as well as chronic versus acute events can explain the difference seen at the mRNA level. Further, acute (*in vitro*) versus chronic condition (*in vivo*) vary in the impact on negative and positive feedback loops in the cells. Further, a phenotype of BMDM is different than that of Kupffer cells.

Nrf2 is a well-known master regulator of HO-1, and the feedback activation of Nrf2 in the absence of HO-1 may provide regulatory mechanism on LNX1 expression; however, we found no correlation with the expression pattern of Nrf2 and phenotype of HO-1-deficient mice in liver fibrosis models. We have further analyzed the expression of ferroptosis-associated genes in our datasets from the RNA-seq in Mϕ (based on the necroptosis markers as in Chen et al. [2021]). There was a mild elevation of *PTGS2* gene in KO at the baseline and in BDL as compared with controls, however no difference in *CHAC1* or *NFE2L2* (encoding Nrf2) or *TFR*, *ASCL4* mRNA expression levels (data not shown).

To determine whether LNX1 is a regulator of HO-1-deficient Mϕ phenotype, we overexpressed *LNX1* in RAW264.7 Mϕ with knockdown of HO-1 and observed a significant elevation of the M2-like polarization markers (CD163, Marco, and CD206) upon treatment with heme. Our data suggest that downregulation of LNX1 in HO-1-deficient Mϕ may promote Notch1 signaling and M1 Mϕ polarization, facilitating liver injury and fibrosis. However, overexpression of *LNX1* does not increase mRNA levels of Notch1, suggesting a LNX1-Numb-regulated posttranslational control of Notch1 activity.

SULT2A8, a sulfotransferase for bile acids, is regulated by PPARα. PPARα is a key target for BLVR-A (Hinds et al., 2016). The expression levels of *BLVR-A* and *SULT2A8* were suppressed in the absence of HO-1 in mice after BDL, suggesting that HO-1 might regulate *SULT2A8* expression via PPARα.

Further, we showed increased GPNMB levels in Mϕ in the HO-1 conditional KO mice in the liver only in fibrotic livers but not in the controls. GPNMB was shown to be upregulated in Mϕ and endothelial cells in response to ischemic injury and is important in phagocytosis involved in wound healing (Li et al., 2010). Indeed, HO-1 in Mϕ was previously linked to improved phagocytosis of bacteria (Wegiel et al., 2014). GPNMB levels were elevated in the CCL4-treated mice within the Mϕ population in the liver (Kumagai et al., 2015). In that model, deletion of GPNMB led to an increase in metalloproteinases 19 (MMP19) and fibrinolysis (Kumagai et al., 2015), suggesting that high expression of GPNMB might be important in regulation of fibrosis driven by HO-1 deficiency in Mϕ. Interestingly, this was accompanied by increased Marco expression, a scavenger receptor class-A protein and innate marker of Mϕ activation and phagocytosis, in HO-1-deficient Mϕ in the livers of control and in BDL-subjected mice. Elevation of Marco and GPNMB in HO-1-deficient Mϕ or in the presence of heme might be a compensation mechanism for attenuated expression of CD163, the scavenger receptor cysteine-rich (SRCR) family class B (Fabriek et al., 2005).

Dysregulated immune responsiveness is central to liver disease and accelerates the development and progression of liver fibrosis (Oates et al., 2019). Our data suggest a critical role of HO-1 in the modulation of liver-associated Mϕ that entails regulating genes involved in oxidative stress metabolism, extracellular matrix organization, and acute inflammatory response. Therefore, HO-1 represents a potential drug target for the prevention or treatment of liver fibrosis. We speculate that the relatively high levels of HO-1 in inflammatory cells or its induction by heme released from dying cells might suppress progression of liver fibrosis. Further, high expression of LNX1 in human liver explants with low levels of HO-1 in patients with cryptogenic cirrhosis may indicate M2-like macrophage switch supporting an established tumor-like immune niche in liver fibrosis patients. High numbers of HO-1$^+$ cells in the NASH patients with low fibrosis stage may indicate a mechanism for halting the progression of disease, which when established is characterized by redistribution of HO-1$^+$ cells into the fibrotic regions. Interestingly, inflammation in PBC livers is also associated with high number of HO-1$^+$ and LNX1$^+$ cells, which both are associated with skewing Mϕ toward M2 phenotype. The association between HO-1 and LNX1 levels should be further validated in the larger cohort of patients as may be valid marker of immune cell niche in NASH and liver fibrosis.

In summary, we have identified LNX1/Notch1 pathway downstream of HO-1-mediated immune regulation in Mϕ using the murine BDL-model of liver fibrosis. HO-1 mediates pro-resolution M2-polarization of Mϕ, protecting liver from excessive ductular reaction and fibrosis, with LNX1 as a key downstream target for HO-1 mediating these effects.

Limitations of the study

Heme metabolism catalyzed by HO-1 generates three active products, including carbon monoxide, bilirubin, and iron. We have not assessed whether any of these products could mitigate liver fibrosis in myeloid-specific *Hmox1* knockout mice. We employed two models of liver fibrosis: surgical and diet-induced liver fibrosis in mice. We cannot exclude the possibility that HO-1 may involve other signaling

pathways at the different stages of liver fibrosis or in other models. Further, we analyzed the late gene expression changes in end-stage liver fibrosis rather than early drivers of liver fibrosis. Our approaches were limited to a single time point of measuring the gene expression levels. Therefore, information about dynamic changes in these genes in macrophages is limited. Further, HO-1 may play a role in multiple cell types beyond myeloid compartment. Finally, a larger number of human specimens will allow for correlation of the levels of HO-1 and LNX1 in various stages of liver fibrosis and NASH.

STAR★METHODS

Detailed methods are provided in the online version of this paper and include the following:

- KEY RESOURCES TABLE
- RESOURCE AVAILABILITY
  - Lead contact
  - Materials availability
  - Data and code availability
- EXPERIMENTAL MODEL AND SUBJECT DETAILS
  - Cells and reagents
  - Animal models
  - NASH model
  - Human tissues and staining
- METHOD DETAILS
  - Cell transfection, plasmids
  - BDL surgery
  - RNA isolation from HA-tagged liver Mϕ
  - Hepatic hydroxyproline determination
  - Immunohistochemistry (IHC) staining
  - Prussian blue staining
  - Immunoblotting
  - RNA extraction and RT-PCR
  - RNA library preparation and sequencing
- QUANTIFICATION AND STATISTICAL ANALYSIS
  - RNA-seq analysis
- STATISTICAL ANALYSIS

SUPPLEMENTAL INFORMATION

Supplemental information can be found online at https://doi.org/10.1016/j.isci.2022.104983.

ACKNOWLEDGMENTS

Our studies were supported in part by the following funding : NCI R21 CA169904, NCI R21 CA256720. NIDDK R01 DK104714 and R01 DK125846, start-up funds from Department of Surgery at BIDMC to BW. G.W. was supported by National Natural Science Foundation of China (No. 82103771). We thank Dr. Mikio Furuse (NIPS, Okazaki, Aichi, Japan) for providing the full-length cDNA of mouse LNX1p80. We thank Drs. Elzbieta Kaczmarek and Jonathan Hecht for fruitful discussions of our work and editing of our manuscript. The graphical scheme was performed using the BioRender software.

AUTHOR CONTRIBUTIONS

G.C., L.F, G.W., Y.V.P., and B.W. designed the study. M.J. performed NASH experiments and western blotting. G.C. did the *RiboTag* assays and RT-PCR, histology analysis. L.J., K.D.S., and P.C. helped with analysis of the *in vitro* experiments. E.C. performed IHC staining. J.A. and L.F. initiated the study and showed the first effects of HO-1 deficiency in BDL model. G.C., L.F., G.W., and J. A. performed surgeries and *in vivo* experiments. I.N. is a pathologist and provided insights into human biopsies analysis. Z.H. performed the RNA-seq and analysis. G.C., Y.V.P, K.D.S, and B.W wrote the paper with input from all authors. S.C.R. provided a guide into liver fibrosis models and edited the paper. B.W. and Y.V.P. supervised the work.

DECLARATION OF INTERESTS

The authors declare no competing interests.

Received: January 24, 2022
Revised: July 1, 2022
Accepted: August 16, 2022
Published: September 16, 2022

REFERENCES

Adams, J.M., and Jafar-Nejad, H. (2019). The roles of Notch signaling in liver development and disease. Biomolecules *9*. https://doi.org/10.3390/biom9100608.

An, P., Wei, L.L., Zhao, S., Sverdlov, D.Y., Vaid, K.A., Miyamoto, M., Kuramitsu, K., Lai, M., and Popov, Y.V. (2020). Hepatocyte mitochondria-derived danger signals directly activate hepatic stellate cells and drive progression of liver fibrosis. Nat. Commun. *11*, 2362. https://doi.org/10.1038/s41467-020-16092-0.

Asimakopoulou, A., Weiskirchen, S., and Weiskirchen, R. (2016). Lipocalin 2 (LCN2) expression in hepatic malfunction and therapy. Front. Physiol. *7*, 430. https://doi.org/10.3389/fphys.2016.00430.

Asrani, S.K., Devarbhavi, H., Eaton, J., and Kamath, P.S. (2019). Burden of liver diseases in the world. J. Hepatol. *70*, 151–171. https://doi.org/10.1016/j.jhep.2018.09.014.

Baisiwala, S., Hall, R.R., 3rd, Saathoff, M.R., M Shireman, J., Park, C., Budhiraja, S., Goel, C., Warnke, L., Hardiman, C., Wang, J.Y., et al. (2020). LNX1 modulates Notch1 signaling to promote expansion of the glioma stem cell population during temozolomide therapy in glioblastoma. Cancers *12*, E3505. https://doi.org/10.3390/cancers12123505.

Barikbin, R., Neureiter, D., Wirth, J., Erhardt, A., Schwinge, D., Kluwe, J., Schramm, C., Tiegs, G., and Sass, G. (2012). Induction of heme oxygenase 1 prevents progression of liver fibrosis in Mdr2 knockout mice. Hepatology *55*, 553–562. https://doi.org/10.1002/hep.24711.

Bisht, K., Canesin, G., Cheytan, T., Li, M., Nemeth, Z., Csizmadia, E., Woodruff, T.M., Stec, D.E., Bulmer, A.C., Otterbein, L.E., and Wegiel, B. (2019). Deletion of biliverdin reductase A in myeloid cells promotes chemokine expression and chemotaxis in part via a complement C5a–C5aR1 pathway. J. Immunol. *202*, 2982–2990. https://doi.org/10.4049/jimmunol.1701443.

Boulter, L., Govaere, O., Bird, T.G., Radulescu, S., Ramachandran, P., Pellicoro, A., Ridgway, R.A., Seo, S.S., Spee, B., Van Rooijen, N., et al. (2012). Macrophage-derived Wnt opposes Notch signaling to specify hepatic progenitor cell fate in chronic liver disease. Nat. Med. *18*, 572–579. https://doi.org/10.1038/nm.2667.

Canesin, G., Di Ruscio, A., Li, M., Ummarino, S., Hedblom, A., Choudhury, R., Krzyzanowska, A., Csizmadia, E., Palominos, M., Stiehm, A., et al. (2020a). Scavenging of labile heme by hemopexin is a key checkpoint in cancer growth and metastases. Cell Rep. *32*, 108181. https://doi.org/10.1016/j.celrep.2020.108181.

Canesin, G., Hejazi, S.M., Swanson, K.D., and Wegiel, B. (2020b). Heme-derived metabolic signals dictate immune responses. Front. Immunol. *11*, 66. https://doi.org/10.3389/fimmu.2020.00066.

Chen, X., Comish, P.B., Tang, D., and Kang, R. (2021). Characteristics and biomarkers of ferroptosis. Front. Cell Dev. Biol. *9*, 637162. https://doi.org/10.3389/fcell.2021.637162.

Cornwell, M., Vangala, M., Taing, L., Herbert, Z., Köster, J., Li, B., Sun, H., Li, T., Zhang, J., Qiu, X., et al. (2018). VIPER: visualization Pipeline for RNA-seq, a Snakemake workflow for efficient and complete RNA-seq analysis. BMC Bioinf. *19*, 135. https://doi.org/10.1186/s12859-018-2139-9.

Dobin, A., Davis, C.A., Schlesinger, F., Drenkow, J., Zaleski, C., Jha, S., Batut, P., Chaisson, M., and Gingeras, T.R. (2013). STAR: ultrafast universal RNA-seq aligner. Bioinformatics *29*, 15–21. https://doi.org/10.1093/bioinformatics/bts635.

Ellis, E.L., and Mann, D.A. (2012). Clinical evidence for the regression of liver fibrosis. J. Hepatol. *56*, 1171–1180. https://doi.org/10.1016/j.jhep.2011.09.024.

Fabriek, B.O., Dijkstra, C.D., and van den Berg, T.K. (2005). The macrophage scavenger receptor CD163. Immunobiology *210*, 153–160. https://doi.org/10.1016/j.imbio.2005.05.010.

Feng, L., Yuen, Y.L., Xu, J., Liu, X., Chan, M.Y., Wang, K., Fong, W.P., Cheung, W.T., and Lee, S.S. (2017). Identification and characterization of a novel PPARα-regulated and 7α-hydroxyl bile acid-preferring cytosolic sulfotransferase mL-STL (Sult2a8). J Lipid Res *58*, 1114–1131.

Froh, M., Conzelmann, L., Walbrun, P., Netter, S., Wiest, R., Wheeler, M.D., Lehnert, M., Uesugi, T., Scholmerich, J., and Thurman, R.G. (2007). Heme oxygenase-1 overexpression increases liver injury after bile duct ligation in rats. World J. Gastroenterol. *13*, 3478–3486. https://doi.org/10.3748/wjg.v13.i25.3478.

Geisler, F., and Strazzabosco, M. (2015). Emerging roles of Notch signaling in liver disease. Hepatology *61*, 382–392. https://doi.org/10.1002/hep.27268.

Hedblom, A., Hejazi, S.M., Canesin, G., Choudhury, R., Hanafy, K.A., Csizmadia, E., Persson, J.L., and Wegiel, B. (2019). Heme detoxification by heme oxygenase-1 reinstates proliferative and immune balances upon genotoxic tissue injury. Cell Death Dis. *10*, 72. https://doi.org/10.1038/s41419-019-1342-6.

Hinds, T.D., Jr., Burns, K.A., Hosick, P.A., McBeth, L., Nestor-Kalinoski, A., Drummond, H.A., AlAmodi, A.A., Hankins, M.W., Vanden Heuvel, J.P., and Stec, D.E. (2016). Biliverdin reductase A attenuates hepatic steatosis by inhibition of glycogen synthase kinase (GSK) 3beta phosphorylation of serine 73 of peroxisome proliferator-activated receptor (PPAR) alpha. J. Biol. Chem. *291*, 25179–25191. https://doi.org/10.1074/jbc.M116.731703.

Keyse, S.M., and Tyrrell, R.M. (1989). Heme oxygenase is the major 32-kDa stress protein induced in human skin fibroblasts by UVA radiation, hydrogen peroxide, and sodium arsenite. Proc. Natl. Acad. Sci. USA *86*, 99–103. https://doi.org/10.1073/pnas.86.1.99.

Kumagai, K., Tabu, K., Sasaki, F., Takami, Y., Morinaga, Y., Mawatari, S., Hashimoto, S., Tanoue, S., Kanmura, S., Tamai, T., et al. (2015). Glycoprotein nonmetastatic melanoma B (Gpnmb)-Positive macrophages contribute to the balance between fibrosis and fibrolysis during the repair of acute liver injury in mice. PLoS One *10*, e0143413. https://doi.org/10.1371/journal.pone.0143413.

Li, B., Castano, A.P., Hudson, T.E., Nowlin, B.T., Lin, S.L., Bonventre, J.V., Swanson, K.D., and Duffield, J.S. (2010). The melanoma-associated transmembrane glycoprotein Gpnmb controls trafficking of cellular debris for degradation and is essential for tissue repair. FASEB J *24*, 4767–4781. https://doi.org/10.1096/fj.10-154757.

Li, L., Grenard, P., Nhieu, J.T.V., Julien, B., Mallat, A., Habib, A., and Lotersztajn, S. (2003). Heme oxygenase-1 is an antifibrogenic protein in human hepatic myofibroblasts. Gastroenterology *125*, 460–469. https://doi.org/10.1016/s0016-5085(03)00906-5.

Llovet, J.M., and Bruix, J. (2008). Novel advancements in the management of hepatocellular carcinoma in 2008. J. Hepatol. *48* (*Suppl 1*), S20–S37. https://doi.org/10.1016/j.jhep.2008.01.022.

Love, M.I., Huber, W., and Anders, S. (2014). Moderated estimation of fold change and dispersion for RNA-seq data with DESeq2. Genome Biol. *15*, 550. https://doi.org/10.1186/s13059-014-0550-8.

Lundvig, D.M.S., Immenschuh, S., and Wagener, F.A.D.T.G. (2012). Heme oxygenase, inflammation, and fibrosis: the good, the bad, and the ugly? Front. Pharmacol. *3*, 81. https://doi.org/10.3389/fphar.2012.00081.

Malaguarnera, L., Madeddu, R., Palio, E., Arena, N., and Malaguarnera, M. (2005). Heme oxygenase-1 levels and oxidative stress-related parameters in non-alcoholic fatty liver disease patients. J. Hepatol. *42*, 585–591. https://doi.org/10.1016/j.jhep.2004.11.040.

Mederacke, I., Hsu, C.C., Troeger, J.S., Huebener, P., Mu, X., Dapito, D.H., Pradere, J.P., and Schwabe, R.F. (2013). Fate tracing reveals hepatic stellate cells as dominant contributors to liver fibrosis independent of its aetiology. Nat. Commun. *4*, 2823. https://doi.org/10.1038/ncomms3823.

Monsalve, E., Pérez, M.A., Rubio, A., Ruiz-Hidalgo, M.J., Baladrón, V., García-Ramírez, J.J., Gómez, J.C., Laborda, J., and Díaz-Guerra, M.J.M. (2006). Notch-1 up-regulation and signaling following macrophage activation modulates gene expression patterns known to affect antigen-presenting capacity and cytotoxic activity. J. Immunol. *176*, 5362–5373.

Naito, Y., Takagi, T., and Higashimura, Y. (2014). Heme oxygenase-1 and anti-inflammatory M2 macrophages. Arch. Biochem. Biophys. *564*, 83–88. https://doi.org/10.1016/j.abb.2014.09.005.

Nemeth, Z., Csizmadia, E., Vikstrom, L., Li, M., Bisht, K., Feizi, A., Otterbein, S., Zuckerbraun, B., Costa, D.B., Pandolfi, P.P., et al. (2016). Alterations of tumor microenvironment by carbon monoxide impedes lung cancer growth. Oncotarget *7*, 23919–23932. https://doi.org/10.18632/oncotarget.8081.

Oates, J.R., McKell, M.C., Moreno-Fernandez, M.E., Damen, M.S.M.A., Deepe, G.S., Jr., Qualls, J.E., and Divanovic, S. (2019). Macrophage function in the pathogenesis of non-alcoholic fatty liver disease: the Mac Attack. Front. Immunol. *10*, 2893. https://doi.org/10.3389/fimmu.2019.02893.

Peng, Z.W., Ikenaga, N., Liu, S.B., Sverdlov, D.Y., Vaid, K.A., Dixit, R., Weinreb, P.H., Violette, S., Sheppard, D., Schuppan, D., and Popov, Y. (2016). Integrin alphavbeta6 critically regulates hepatic progenitor cell function and promotes ductular reaction, fibrosis, and tumorigenesis. Hepatology *63*, 217–232. https://doi.org/10.1002/hep.28274.

Popov, Y., Patsenker, E., Stickel, F., Zaks, J., Bhaskar, K.R., Niedobitek, G., Kolb, A., Friess, H., and Schuppan, D. (2008). Integrin alphavbeta6 is a marker of the progression of biliary and portal liver fibrosis and a novel target for antifibrotic therapies. J. Hepatol. *48*, 453–464. https://doi.org/10.1016/j.jhep.2007.11.021.

Raffaele, M., Carota, G., Sferrazzo, G., Licari, M., Barbagallo, I., Sorrenti, V., Signorelli, S.S., and Vanella, L. (2019). Inhibition of heme oxygenase antioxidant activity exacerbates hepatic steatosis and fibrosis in vitro. Antioxidants *8*, E277. https://doi.org/10.3390/antiox8080277.

Salley, T.N., Mishra, M., Tiwari, S., Jadhav, A., and Ndisang, J.F. (2013). The heme oxygenase system rescues hepatic deterioration in the condition of obesity co-morbid with type-2 diabetes. PLoS One *8*, e79270. https://doi.org/10.1371/journal.pone.0079270.

Sanchez, M., Galy, B., Schwanhaeusser, B., Blake, J., Bähr-Ivacevic, T., Benes, V., Selbach, M., Muckenthaler, M.U., and Hentze, M.W. (2011). Iron regulatory protein-1 and -2: transcriptome-wide definition of binding mRNAs and shaping of the cellular proteome by iron regulatory proteins. Blood *118*. e168–179. https://doi.org/10.1182/blood-2011-04-343541.

Sanz, E., Yang, L., Su, T., Morris, D.R., McKnight, G.S., and Amieux, P.S. (2009). Cell-type-specific isolation of ribosome-associated mRNA from complex tissues. Proc. Natl. Acad. Sci. USA *106*, 13939–13944. https://doi.org/10.1073/pnas.0907143106.

Stec, D.E., and Hinds, T.D., Jr. (2020). Natural product heme oxygenase inducers as treatment for nonalcoholic fatty liver disease. Int. J. Mol. Sci. *21*, E9493. https://doi.org/10.3390/ijms21249493.

Tag, C.G., Sauer-Lehnen, S., Weiskirchen, S., Borkham-Kamphorst, E., Tolba, R.H., Tacke, F., and Weiskirchen, R. (2015). Bile duct ligation in mice: induction of inflammatory liver injury and fibrosis by obstructive cholestasis. J Vis Exp. https://doi.org/10.3791/52438.

Takahashi, S., Iwamoto, N., Sasaki, H., Ohashi, M., Oda, Y., Tsukita, S., and Furuse, M. (2009). The E3 ubiquitin ligase LNX1p80 promotes the removal of claudins from tight junctions in MDCK cells. J. Cell Sci. *122*, 985–994. https://doi.org/10.1242/jcs.040055.

Tanaka, H., Matsumura, I., Nakajima, K., Daino, H., Sonoyama, J., Yoshida, H., Oritani, K., Machii, T., Yamamoto, M., Hirano, T., and Kanakura, Y. (2000). GATA-1 blocks IL-6-induced macrophage differentiation and apoptosis through the sustained expression of cyclin D1 and bcl-2 in a murine myeloid cell line M1. Blood *95*, 1264–1273.

Tsuchida, T., and Friedman, S.L. (2017). Mechanisms of hepatic stellate cell activation. Nat. Rev. Gastroenterol. Hepatol. *14*, 397–411. https://doi.org/10.1038/nrgastro.2017.38.

Tsui, T.Y., Lau, C.K., Ma, J., Glockzin, G., Obed, A., Schlitt, H.J., and Fan, S.T. (2006). Adeno-associated virus-mediated heme oxygenase-1 gene transfer suppresses the progression of micronodular cirrhosis in rats. World J. Gastroenterol. *12*, 2016–2023. https://doi.org/10.3748/wjg.v12.i13.2016.

Vijayan, V., Wagener, F.A.D.T.G., and Immenschuh, S. (2018). The macrophage heme-heme oxygenase-1 system and its role in inflammation. Biochem. Pharmacol. *153*, 159–167. https://doi.org/10.1016/j.bcp.2018.02.010.

Wang, Q.M., Du, J.L., Duan, Z.J., Guo, S.B., Sun, X.Y., and Liu, Z. (2013). Inhibiting heme oxygenase-1 attenuates rat liver fibrosis by removing iron accumulation. World J. Gastroenterol. *19*, 2921–2934. https://doi.org/10.3748/wjg.v19.i19.2921.

Wegiel, B., Baty, C.J., Gallo, D., Csizmadia, E., Scott, J.R., Akhavan, A., Chin, B.Y., Kaczmarek, E., Alam, J., Bach, F.H., et al. (2009). Cell surface biliverdin reductase mediates biliverdin-induced anti-inflammatory effects via phosphatidylinositol 3-kinase and Akt. J. Biol. Chem. *284*, 21369–21378. https://doi.org/10.1074/jbc.M109.027433.

Wegiel, B., Hanto, D.W., and Otterbein, L.E. (2013). The social network of carbon monoxide in medicine. Trends Mol. Med. *19*, 3–11. https://doi.org/10.1016/j.molmed.2012.10.001.

Wegiel, B., Hauser, C.J., and Otterbein, L.E. (2015). Heme as a danger molecule in pathogen recognition. Free Radic. Biol. Med. *89*, 651–661. https://doi.org/10.1016/j.freeradbiomed.2015.08.020.

Wegiel, B., Larsen, R., Gallo, D., Chin, B.Y., Harris, C., Mannam, P., Kaczmarek, E., Lee, P.J., Zuckerbraun, B.S., Flavell, R., et al. (2014). Macrophages sense and kill bacteria through carbon monoxide-dependent inflammasome activation. J. Clin. Invest. *124*, 4926–4940. https://doi.org/10.1172/JCI72853.

Wei, G., An, P., Vaid, K.A., Nasser, I., Huang, P., Tan, L., Zhao, S., Schuppan, D., and Popov, Y.V. (2020a). Comparison of murine steatohepatitis models identifies a dietary intervention with robust fibrosis, ductular reaction, and rapid progression to cirrhosis and cancer. Am. J. Physiol. Gastrointest. Liver Physiol. *318*, G174–G188. https://doi.org/10.1152/ajpgi.00041.2019.

Wei, G., Cao, J., Huang, P., An, P., Badlani, D., Vaid, K.A., Zhao, S., Wang, D.Q.H., Zhuo, J., Yin, L., et al. (2020b). Synthetic human ABCB4 mRNA therapy rescues severe liver disease phenotype in a BALB/c.Abcb4(-/-) mouse model of PFIC3. J. Hepatol. *74*, 1416–1428. https://doi.org/10.1016/j.jhep.2020.12.010.

Weijzen, S., Velders, M.P., Elmishad, A.G., Bacon, P.E., Panella, J.R., Nickoloff, B.J., Miele, L., and Kast, W.M. (2002). The Notch ligand Jagged-1 is able to induce maturation of monocyte-derived human dendritic cells. J. Immunol. *169*, 4273–4278.

Williams, R., Alexander, G., Armstrong, I., Baker, A., Bhala, N., Camps-Walsh, G., Cramp, M.E., de Lusignan, S., Day, N., Dhawan, A., et al. (2018). Disease burden and costs from excess alcohol consumption, obesity, and viral hepatitis: fourth report of the Lancet Standing Commission on Liver Disease in the UK. Lancet *391*, 1097–1107. https://doi.org/10.1016/S0140-6736(17)32866-0.

Zhang, M., Nakamura, K., Kageyama, S., Lawal, A.O., Gong, K.W., Bhetraratana, M., Fujii, T., Sulaiman, D., Hirao, H., Bolisetty, S., et al. (2018). Myeloid HO-1 modulates macrophage polarization and protects against ischemia-reperfusion injury. JCI Insight *3*, 120596. https://doi.org/10.1172/jci.insight.120596.

STAR★METHODS

KEY RESOURCES TABLE

REAGENT or RESOURCE	SOURCE	IDENTIFIER
Antibodies		
Anti-HA (HA.11)	Biolegend	Cat#: 901,514; RRID: AB_2565336
Anti-E-Cadherin	Cell Signaling	Cat#: 24E10
Anti-CK-19	Abcam	Cat#: Ab18586
Rabbit polyclonal anti-HO1	Enzo Laboratories	Cat#: ADI-OSA-110; RRID:AB_10617276
Notch1	Proteintech	Cat#: 20687-1-AP
Anti-Total Notch1	Novus Biologicals	Cat#: NBP-78292
Goat polyclonal anti-Jagged1	Santa Cruz Biotechnology	Cat#: sc-6011
Mouse monoclonal anti-HO-1	Enzo Laboratories	Cat#: ADI-OSA-110; RRID:AB_10617276
Mouse monoclonal anti-Beta-Actin	Sigma Aldrich	Cat#: A2228; RRID:AB_476697
Anti-Nrf2 (D1Z9C) Rabbit mAb	Cell Signaling Technology	Cat#: 12721S
Mouse Anti-LNX-1	Sigma Aldrich	Cat #: AV43367-100UL
Rabbit anti-Mouse Aconitase 1 Polyclonal Antibody	MYBIOSOURCE LLC	Cat#: MBS2028596
Biological samples		
Liver Biopsies from NAFLD patients	Pathology/BIDMC	N/A
Human liver explants	Heidelberg University	Peng et al. (2016)
Chemicals, peptides, and recombinant proteins		
Macrophage Colony Stimulating Factor Human Recombinant (M-CSF)	Prospec	Cat # CYT-308
Hemin	Sigma-Aldrich	Cat # 51,280
RNasin	Promega	Cat #N2111
Protease Inhibitor Cocktail	Sigma-Aldrich	Cat #P8849
Complete™, Mini Protease Inhibitor Cocktail	Roche	Cat # 11,836,153,001
Critical commercial assays		
RNeasy Plus Mini Kits	Qiagen	Cat # 74,034
BCA Protein Kit	Pierce	Cat# 23,227
SuperSignal™ West Pico PLUS Chemiluminescent Substrate	Thermo Fisher	Cat #: 34,580
SuperSignal™ West Femto Maximum Sensitivity Substrate	Thermo Fisher	Cat #: 34,095
Deposited data		
RNA sequencing data	This paper	GEO Submission (GSE206069)
Experimental models: Cell lines		
RAW 264.7	ATCC	TIB-71
RAW 264.7-mirHO-1	Wegiel et al. (2014)	N/A
RAW 264.7-mirC	Wegiel et al. (2014)	N/A
Experimental models: Organisms/strains		
LysM-Cre:Hmox$^{fl/fl}$	Wegiel et al. (2014).	N/A
Hmox1$^{fl/fl}$	Wegiel et al. (2014).	N/A
B6J.129(Cg)-*Rpl22*$^{tm1.1Psam}$/SjJ	Jackson Laboratories	Strain #:029,977

(*Continued on next page*)

Continued

REAGENT or RESOURCE	SOURCE	IDENTIFIER
Oligonucleotides		
Beta-Actin FW: CCACGGATTCCATACCCAAGA	This paper	N/A
Beta-Actin RV: TAGACTTCGAGCAGGAGATGG	This paper	N/A
Collagen-I FW: TACAGCACGCTTGTGGATG	This paper	N/A
Collagen-I RV: TTGGGATGGAGGGAGTTTA	This paper	N/A
TGF-beta FW: TGAACCAAGGAGACGGAATACAGG	This paper	N/A
TGF-beta RV: GCCATGAGGAGCAGGAAGGG	This paper	N/A
Acta2 FW: ACTGGGACGACATGGAAAAG	This paper	N/A
Acta2 RV: GTTCAGTGGTGCCTCTGTCA	This paper	N/A
Hmox1 FW: CAGGATTTGTCAGAGGCCCTGAAGG	Canesin et al. (2020a)	N/A
Hmox1 RV: TGTGGTACAGGGAGGCCATCACC	Canesin et al. (2020b)	N/A
BLVR-A FW: ATTTCTGCCACCATGGAAAA	This paper	N/A
BLVR-A RV: CTCCAAGGACCCAGATTTGA	This paper	N/A
Hemopexin FW: CCTGACAAAGGGAGGCAATA	This paper	N/A
Hemopexin RV: TCTTGGCTGCATTCAGTTTG	This paper	N/A
iNOS FW: CAGCTGGGCTGTACAAACCTT	This paper	N/A
iNOS RV: CATTGGAAGTGAAGCGGTTCG	This paper	N/A
CD206 FW: TCTTTGCCTTTCCCAGTCTCC	This paper	N/A
CD206 RV: TGACACCCAGCGGAATTTC	This paper	N/A
CD163 FW: GAAGCCTTGACAGGACAGCC	This paper	N/A
CD163 RV: CATAATGAGACCCTATTGCGAAC	This paper	N/A
LNX1 FW: ATGGTGAGCCAGTAGCCAAC	This paper	N/A
LNX1 RV: CTTGGGAAGACTTCGGGGAC	This paper	N/A
LCN2 FW: CCAGTTCGCCATGGTATTTT	This paper	N/A
LCN2 RV: GGTGGGGACAGAGAAGATGA	This paper	N/A
SULT2A8 FW: AGGAACCCACTGGTTGAATG	This paper	N/A
SULT2A8 RV: GAAGGAGAGAGGCCATGAGA	This paper	N/A
GPNMB FW: GTGTCCTGATCTCCATCGGC	This paper	N/A
GPNMB RV: GCGTGACTGAGGAGAACACT	This paper	N/A
MARCO FW: GATGTGCTGTGGCAATGGAT	This paper	N/A
MARCO RV: CTGGAGAGCCTCGTTCACCT	This paper	N/A
CD14 FW: CTGATCTCAGCCCTCTGTCC	This paper	N/A
CD14 RV: GCTTCAGCCCAGTGAAAGAC	This paper	N/A
NOTCH1 FW: TCAGGGTGTCTTCCAGATCC	This paper	N/A
NOTCH1 RV: CAGCATCCACATTGTTCACC	This paper	N/A
HES1 FW: CTACCCCAGCCAGTGTCAAC	This paper	N/A
HES1 RV: ATGCCGGGAGCTATCTTTCT	This paper	N/A
GATA1 FW: GATGGAATCCAGACGAGGAA	This paper	N/A
GATA1 RV: GCCCTGACAGTACCACAGGT	This paper	N/A
CD11b FW: accgtgtccaaagcttggtt	This paper	N/A
CD11b RV: atcagcgtccatgtccacag	This paper	N/A
MRC-1 (CD206) FW: TCTTTGCCTTTCCCAGTCTCC	This paper	N/A
MRC-1 (CD206) RV: TGACACCCAGCGGAATTTC	This paper	N/A

(*Continued on next page*)

Continued

REAGENT or RESOURCE	SOURCE	IDENTIFIER
IL6 FW: GCCAGCTATGAACTCCTTCT	This paper	N/A
IL6 RV: GAAGGCAGCAGGCAACAC	This paper	N/A
Recombinant DNA		
Mammalian expression vector of N-terminal HA-tagged mouse NLX1p80	Dr. Mikio Furuse, NIPS, Okazaki, Japan. (Takahashi et al., 2009).	N/A
Software and algorithms		
Differential gene expression analysis (DESeq2, v1.22.1)	This paper	GEO Submission (GSE206069)
RNA Sequencing analysis (VIPER snakemake pipeline)	This paper	GEO Submission (GSE206069)

RESOURCE AVAILABILITY

Lead contact

Further information and requests for resources and reagents should be directed to and will be fulfilled by the Lead Contact, Dr. Barbara Wegiel (Department of Surgery, Beth Israel Deaconess Medical Center, Harvard Medical School, bwegiel@bidmc.harvard.edu).

Materials availability

This study did not generate any unique reagents.

Data and code availability

- RNA-seq data have been deposited at GEO (GSE206069) and are publicly available as of the date of publication. Accession numbers are listed in the Key resources table.
- This paper does not report original code.
- Any additional information required to reanalyze the data reported in this paper is available from the lead contact upon request.

EXPERIMENTAL MODEL AND SUBJECT DETAILS

Cells and reagents

The murine macrophage cell line RAW 264.7 was grown in RPMI supplemented with 10% fetal bovine serum and 1% antibiotics (Gibco). Stable HO-1 knocked-down cells (mirHO-1) and control cells (mirC) were employed (Wegiel et al., 2014).

Primary bone marrow derived macrophages (BMDMs) were isolated from female and male mice (7-10 weeks of age) and differentiated for 5-6 days (Wegiel et al., 2009). Briefly, BM cells were isolated from the mouse femurs and were differentiated for five days in M-CSF medium (RPMI containing: 20 ng/mL mouse recombinant M-CSF (ProSpec), 15% fetal bovine serum (Thermo Scientific), 1% antibiotics and antifungal solution (Gibco). Fresh M-CSF medium was added to cells at day 3 of culture. Where indicated, BMDM were treated with heme (1-50 μM) for 24 h.

Heme (Sigma-Aldrich) was prepared by dissolving powder in 0.1 N NaOH and then titrated with 0.1 N HCl to biological pH 7.4, followed by adjustment to the final concentration (10 mM) with saline (Canesin et al., 2020a). Heme stock was then aliquoted and frozen at −80°C until use; each aliquot was thawed only once. Experiments utilizing heme were carried out in the dark.

Animal models

All experimental procedures were performed in accordance with relevant guidelines and regulations. All experiments were approved by the Institutional Animal Committee (IACUC) at BIDMC. Animals with conditional macrophage deletion of HO-1 (*LysM-Cre:Hmox1*$^{fl/fl}$) and control mice (*Hmox1*$^{fl/fl}$) are bred in our colony (Hedblom et al., 2019). Mice with conditional deletion of HO-1 in myeloid cells and concomitant

myeloid-specific ribosome epitope-tagging (*LysM-Cre:Hmox1*$^{fl/fl}$*:RiboTag* mice) were obtained by crossing *LysM-Cre:RiboTag* mice (Jackson Laboratories) (Sanz et al., 2009) to *Hmox1*$^{fl/fl}$ mice. *LysM-Cre:RiboTag* were used as controls. Female and male mice (7-10 weeks old) were used *for in vivo* and *in vitro* experiments, and no difference in the responses were noted.

NASH model

All experiments were approved by the Institutional Animal Committee (IACUC) at BIDMC. Female and male mice (7-9 weeks old) were fed irradiated Methionine/Choline deficient (MCD, Envigo, TD.90262) diet for 3 weeks. Liver tissues were collected and processed for H&E and Sirius Red staining. Fibrosis score (0-3) was based on the level of pericellular fibrosis regions: 0- negative, 1-low, 2-medium, 3- high levels. Fatty liver scores (0-3) were based on two sections from the liver: 0- negative, 1- low levels of fat accumulation in one section, 2- strongly positive one section of the liver, 3- both sections strongly positive.

Human tissues and staining

All studies were approved by Committee on Clinical Investigation (IRB) at BIDMC and Heidelberg University (Popov et al., 2008). BIDMC studies were approved as an NIH exemption # 4. Liver biopsies from n = 5 patients with various stages of NAFLD/NASH were pulled from the archival pathology specimens at BIDMC with the following clinical records:

#1: Fibrosis stage: 0, NAS: 7 (Male, 50 years old) and a mild inflammation

#2: Fibrosis stage: 1, NAS: 8 (Female, 51 years old) and a moderate inflammation

#3: Fibrosis stage: 1-2, NAS: 4 (Male, 53 years old) and a mild inflammation

#4: Fibrosis stage: 3, NAS: 3 (Female, 61 years old) and a moderate inflammation

#5: Fibrosis stage: 3-4, NAS: 0 (Male, 52 years old) and a mild inflammation

Thirteen human liver explants were obtained from patients undergoing orthotopic liver transplantation due to end-stage liver disease of various etiologies (n = 3 PBC, n = 5 Alc, n = 5 Crypt) (Peng et al., 2016). The formalin-fixed, paraffin-embedded tissue blocks were sectioned and stained for HO-1 and LNX1 (Bisht et al., 2019).

METHOD DETAILS

Cell transfection, plasmids

The mammalian expression vector of N-terminal HA-tagged mouse LNX1p80 was a kind gift from Dr. Mikio Furuse (NIPS, Okazaki, Japan) (Takahashi et al., 2009). The pCMV vector was used as a control. One or two μg plasmid was transfected into RAW264.7 cells using Lipofectamine 2000. Twenty four to 48 h h later, transfected cells were treated with heme for 6 h.

BDL surgery

All experiments were approved by the Institutional Animal Committee (IACUC) at BIDMC. Male and female mice (7-9 weeks old) were anesthetized with ketamine/xylazine and the abdomen was shaved and washed with alcohol solution, then iodine solution. A midline laparotomy incision, measuring approximately 1–1.5 cm, was performed, the abdominal cavity was opened and 2 sterile retractors were placed for surgical exposure. The bile duct was identified using the surgical microscope, and gently separated from surrounding connective tissue, using blunt forceps. Two ligatures were placed (6-0 silk ligature) proximal to the pancreatic duct with 1–2 mm distance from each other, and secured with two surgical knots. The retractors were removed and 300 μL warm saline solution was administered intraperitoneally before the abdomen was closed in two layers by standard suture. Animals recovered in their cages on the heating pads in the procedure room with water gel and food. Buprenorphine (5 mg/kg) was administered 20 min prior to skin closure, and daily for 48 h post-surgery.

RNA isolation from HA-tagged liver Mϕ

RNA was isolated from HA-tagged liver Mϕ by tissue homogenization and immunoprecipitation (IP) (Sanz et al., 2009). Liver tissues were disrupted in homogenization buffer (50 mM Tris, pH 7.5, 100 mM KCl, 12 mM MgCl2, 1% Nonidet P-40, 1 mM DTT, 200 U/mL Promega RNasin, 1 mg/mL heparin, 100 μg/mL

cycloheximide, Sigma protease inhibitor mixture) and homogenized samples were then centrifuged at 10,000g for 10 min at 4°C. From the resulting supernatant, 80 to 100 μL of sample was used as an input (total liver lysate), while the remaining volume of supernatant (approximately 600 μL) was transferred to a new tube and used for immunoprecipitation. For inputs, 350 μL RLT buffer with β-mercaptoethanol was added and RNA was extracted using RNeasy Plus Mini Kits (Qiagen, Valencia, CA), according to manufacturer's instructions. For IP, 5 μL mouse monoclonal anti-HA antibody (HA.11, BioLegend) was added to each tube and samples were incubated on a rotator at 4°C for 4 h. Samples were then added to a new tube containing 180 μL of previously equilibrated protein A/C magnetic beads (Santa Cruz Biotechnology) and rotated overnight at 4°C. The following day, samples were washed three times for 5 min in High Salt Buffer (50 mM Tris, pH 7.5, 300 mM KCl, 12 mM MgCl2, 1% Nonidet P-40, 1 mM DTT, 100 μg/mL cycloheximide) and 350 μL RLT buffer with β-mercaptoethanol was added to disrupt the antibody-bead-protein bond. Samples were vortexed for 30 s and centrifuged at 10,000 x g for 10 min at 4°C. Supernatants were collected and used for further RNA extraction using RNeasy Plus Mini Kits (Qiagen, Valencia, CA), according to manufacturer's instructions.

Hepatic hydroxyproline determination

Collagen content was determined as relative hydroxyproline (μg/g liver) in 100- to 200-mg liver samples after hydrolysis in 6 N HCl for 16 h at 110°C, as described (Wei et al., 2020b). Total hydroxyproline (mg/whole liver) was calculated based on the individual liver weight and the corresponding relative hydroxyproline content.

Immunohistochemistry (IHC) staining

Tissue samples were formalin fixed followed by paraffin embedding and immunostaining of 5 μm sections was performed (Bisht et al., 2019). Briefly, sections were processed for antigen retrieval with high-pressure cooking in citrate buffer for 1 h. Sections were then blocked for 30 min in 7% horse serum (Vector Laboratories, Burlingame, CA). Primary antibody was then applied to the sections overnight at 4°C. The following day, sections were incubated with biotin-labeled secondary antibody (Vector Laboratories) for 1 h at room temperature, followed by VECTASTAIN Elite ABC kit and detection with ImmPACT DAB (Vector Laboratories). The following primary antibodies were used: to E-cadherin (Cell Signaling, MA), CK-19 (BD Biosciences), HO-1 (Enzo Laboratories), and Notch1 (Proteintech). Hematoxylin and eosin staining was performed as reported before (Nemeth et al., 2016). All images were captured using a Nikon Eclipse E600 microscope (Nikon Instruments, Melville, NY). Connective tissue was stained with Sirius red (Tag et al., 2015) using paraffin-embedded livers. Briefly, 1% direct red in saturated picric acid solution was applied on the de-paraffinized 5 μm sections followed by the de-staining in 1% acetic acid. The slides were mounted in the mounting medium. Images were quantified by counting the number of cells with positive staining in each field of view (three to four sections per animal).

Prussian blue staining

Prussian Blue reaction (Polysciences, Inc., Warrington PA, cat# 24,199) was performed following manufacturer's protocol. Briefly, equal amounts of solution A (4% Potassium Ferrocyanide) and solution B (4% Hydrocloric acid) were applied on formalin-fixed paraffin-embedded tissues for 10 min twice. The tissues were then rinsed in water and stain in solution C (Nuclear Fast Red) for 5 min.

Immunoblotting

Cell lysates were prepared in ice-cold RIPA buffer (50 mM Tris-HCl [pH7.4], 50 mM sodium fluoride, 150 mM NaCl, 1% Nonidet P-40, 0.5 M EDTA [pH 8]) supplemented with the protease inhibitor mixture Complete Mini (Roche, Indianapolis, IN). Samples were centrifuged at 14,000 g at 4°C for 20 min, and supernatants were collected. Protein concentrations of supernatants were measured using a BCA Protein Assay Kit (Thermo Fisher Scientific, Tewksbury, MA). Forty micrograms of each protein sample were then electrophoresed on NuPAGE 4–12% Bis-Tris gel (Life Technologies) in NuPAGE MES SDS Running Buffer (Life Technologies) for 90 min at 100 V. The membranes were blocked with 5% nonfat dry milk in 1x TBS (Boston Bio Products, Ashland, MA) for 1 h and then probed with the appropriate primary antibody (diluted at 1:1000 in 1x TBS with 5% nonfat milk) overnight at 4°C. Membranes were then washed in 1x TBS buffer and incubated with an HRP-conjugated secondary antibody diluted 1:5000 in 1x TBS with 5% nonfat milk for 1 h at room temperature. Membranes were visualized using Super Signal West Pico Chemiluminescent Substrate (Thermo Fisher Scientific) or Femto Maximum Sensitivity Substrate (Thermo Fisher Scientific). We

used the following primary antibodies to: HO-1 (Enzo Laboratories), IRP1/Aco1 (Aconitase 1) (MyBiosource), Nrf2 (Cell Signaling Technology), LNX1 (Sigma Aldrich), and β-Actin (Sigma Aldrich).

RNA extraction and RT-PCR

Total RNA was isolated from cultured cells using RNeasy Plus Mini Kits (QIAGEN, Valencia, CA), and qPCR (Sybr Green Master Mix, Thermo Fisher Scientific) was performed following the cDNA synthesis (HiFiScript Kit) (Bisht et al., 2019). Primers were purchased from Thermo Fisher Scientific. The following oligonucleotides were used for: β-actin - Forward 5′-CCACGGATTCCATACCCAAGA-3′ and Reverse 5′-TAGACTTC GAGCAGGAGATGG-3′; Collagen-I - Forward 5′-TACAGCACGCTTGTGGATG-3′ and Reverse 5′-TTGG GATGGAGGGAGTTTA-3′; TGF-β - Forward 5′-TGAACCAAGGAGACGGAATACAGG-3′ and Reverse 5′-G CCATGAGGAGCAGGAAGGG-3′; Acta-2 - Forward 5′-ACTGGGACGACATGGAAAAG-3′ and Reverse 5′-GTTCAGTGGTGCCTCTGTCA-3′; Hmox1 - Forward 5′-CAGGATTTGTCAGAGGCCCTGAAGG-3′ and Rev erse 5′-TGTGGTACAGGGAGGCCATCACC-3′; BLVR-A - Forward 5′-ATTTCTGCCACCATGGAAAA-3′ and Reverse 5′-CTCCAAGGACCCAGATTTGA-3′; Hemopexin - Forward 5′-CCTGACAAAGGGAGGCAATA-3′ and Reverse 5′-TCTTGGCTGCATTCAGTTTG-3′; iNOS - Forward 5′-CAGCTGGGCTGTACAAACCTT-3′ an d Reverse 5′-CATTGGAAGTGAAGCGGTTCG-3′; CD206 Forward 5′-TCTTTGCCTTTCCCAGTCTCC-3′ and Reverse 5′-TGACACCCAGCGGAATTTC-3′; CD163 Forward 5′-GAAGCCTTGACAGGACAGCC-3′ and Reverse 5′-CATAATGAGACCCTATTGCGAAC-3′; LNX1 - Forward 5′-ATGGTGAGCCAGTAGCCAA C-3′ and Reverse 5′-CTTGGGAAGACTTCGGGGAC-3′; LCN2 - Forward 5′-CCAGTTCGCCATGGTAT TTT-3′ and Reverse 5′-GGTGGGGACAGAGAAGATGA-3′; SULT2A8 - Forward 5′-AGGAACCCACTGGTT GAATG-3′ and Reverse 5′-GAAGGAGAGAGGCCATGAGA-3′; GPNMB - Forward 5′-GTGTCCTGATCTC CATCGGC-3′ and Reverse 5′-GCGTGACTGAGGAGAACACT-3′; MARCO - Forward 5′-GATGTGCTGTGG CAATGGAT-3′ and Reverse 5′-CTGGAGAGCCTCGTTCACCT-3′; CD14 - Forward 5′-CTGATCTCAGCC CTCTGTCC-3′ and Reverse 5′-GCTTCAGCCCAGTGAAAGAC-3′; NOTCH1 - Forward 5′-TCAGGGTG TCTTCCAGATCC-3′ and Reverse 5′-CAGCATCCACATTGTTCACC-3′; Hes1 - Forward 5′-CTACCCCAGC CAGTGTCAAC-3′ and Reverse 5′-ATGCCGGGAGCTATCTTTCT-3′; GATA1 - Forward 5′-GATGGAATC CAGACGAGGAA-3′ and Reverse 5′-GCCCTGACAGTACCACAGGT-3′.

The following program was applied: 95°C for 10 min, 94°C for 30 s, 60°C for 55 s, 72°C for 1 min, 95°C for 1 min, 55°C for 30 s, and 95°C for 30 s (steps #2 to #4 repeated for 40 cycles). Standard software of Stratagene MxPro 3005P version 4.10 (Agilent Technologies, Santa Clara, CA) was used to calculate relative changes in mRNA levels that were normalized to the β-actin levels.

RNA library preparation and sequencing

RNA libraries were prepared from 100 ng of RNA using Roche Kapa Biosystems RiboErase and RNA HyperPrep sample preparation kits. RNA samples were fragmented at 94°C for 8 min with 14 cycles of PCR postadapter ligation, according to manufacturer's recommendation. The finished dsDNA libraries were quantified by Qubit fluorometer and Agilent TapeStation 2200. Libraries were pooled in equimolar ratios and evaluated for cluster efficiency and pool balance with shallow sequencing on an Illumina MiSeq. Final sequencing was performed on an Illumina NovaSeq with paired-end 50 bp reads at the Dana-Farber Cancer Institute Molecular Biology Core Facilities.

QUANTIFICATION AND STATISTICAL ANALYSIS

RNA-seq analysis

Sequenced reads were aligned to the UCSC m10 reference genome assembly and gene counts were quantified using STAR (v2.7.3a) (Dobin et al., 2013). Differential gene expression testing was performed by DESeq2 (v1.22.1) (Love et al., 2014). RNA-seq analysis was performed using the VIPER snakemake pipeline (Cornwell et al., 2018).

STATISTICAL ANALYSIS

All data are reported as mean ± SEM or mean ± SD *In vitro* experiments were performed at least 3 times in triplicate. All statistical analyses were performed using Graph Pad Prism software (GraphPad Prism version 5c, La Jolla, California, USA) and statistical significance was determined using Student's *t* test or one-way or two-way ANOVA with post hoc Tukey's/Dunn's test or Mann–Whitney U test.